AFOSR-TR-97-0662

REPORT DOCUMENTATION PAGE

1. AGENCY USE ONLY (Leave blank)	2. REPORT DATE	3. REPORT TYPE AND DATES COVERED
	9-Jun-97	Final Report for 11/1/93 to 6/30/97

4. TITLE AND SUBTITLE
3D Collapse Phenomena in Dispersive Nonlinear Media: A Critique of Envelope Models

5. FUNDING NUMBERS
AFOSR Grant No. F49620-94-1-0051

6. AUTHOR(S)
A. C. Newell, J.V. Moloney, E.Wright

7. PERFORMING ORGANIZATION NAME(S) AND ADDRESS(ES)
Department of Mathematics
University of Arizona
Tucson, Arizona 85721

8. PERFORMING ORGANIZATION REPORT NUMBER

9. SPONSORING /MONITORING AGENCY NAMES(S) AND ADDRESS(ES)
Air Force Office of Scientific Research/PKA
Bolling AFB, DC 20331-0001

nm

10. SPONSORING/MONITORING AGENCY REPORT NUMBER

11. SUPPLEMENTARY NOTES

12a. DISTRIBUTION/AVAILABILITY STATEMENT
Approved for public release; distribution unlimited.

12b. DISTRIBUTION CODE

13. ABSTRACT (Maximum 200 words)

The main goal of the research was to perform a systematic investigation and evaluation of the utility of envelope equations, in particular, the nonlinear Schroedinger equation (NLS) and its generatizations, for modelling self-focusing (SF) collapse phenomena in transparent dielectric media. The work was successfully carried to completion. We (1) developed a theory of critical collapse for pulses in the presence of normal GVD, (2) developed reliable models for ultrashort pulse propagation in water as a model for propagation inthe vitreaous humor, specifically for propagation in water which accounts for self-focusing collapse, normal GVD, multi-photon absorption and avalanche breakdown and (3) investigated nonlinear reflection properties and have discovered a new phenomenon, the Nonlinear Optical Skin Effect (NOSE) in which a short pulse reflected from the nonlinear absorber suffers a Doppler shift resulting from a moving boundary induced in the medium.

14. SUBJECT TERMS	15. NUMBER OF PAGES
	28
	16. PRICE CODE

17. SECURITY CLASSIFICATION OF REPORT	18. SECURITY CLASSIFICATION	19. SECURITY CLASSIFICATION OF ABSTRACT	20. LIMITATION OF ABSTRACT
UNCLASSIFIED	UNCLASSIFIED	UNCLASSIFIED	UL

Final Technical Report for 1993-1996 on Contract F49620-94-1-0051:

3D Collapse Phenomena in Dispersive Nonlinear Media: A Critique of Envelope Models

Principal Investigators: A.C. Newell, J.V. Moloney
Arizona Center for Mathematical Sciences, Department of Mathematics
University of Arizona, Tucson 85721

Co-Principal Investigator: E.M. Wright
Arizona Center for Mathematical Sciences and Optical Sciences Center
University of Arizona, Tucson 85721

Overview

The main goal of our funded research was to perform a systematic investigation and evaluation of the utility of envelope equations, in particular the nonlinear Schrödinger equation (NLS) and its generalizations, for modelling self-focusing (SF) collpase phenomena in transparent dielectric media. The relevance of this work for the mission of the Air Force is that envelope equations are now being used as models for ultrashort pulse eye damage studies and it is a priori unclear whether these equations are valid. Specifically, for the high peak powers present in ultrashort (sub-picosecond) laser pulses the peak power may exceed the critical power for spatial self-focusing collapse in the vitreous humor (1 MW), resulting in potentially increased retinal damage due to both increased local intensities at the retina and also the occurence of light-induced breakdown (LIB). It is well known that for peak powers exceeding the critical power for self-focusing the envelope equations predict that the field will collapse to a singularity in a finite distance, thus clearly violating the assumptions underlying the envelope approximation. On the other hand other physical effects occuring within the vitreous humor, such as multi-photon absorption (MPA), serve to oppose the collapse and act as perturbations to the envelope equations. The issue is then whether the perturbed or generalized envelope equations avoid the unphysical collapse and are therefore legitimate models for eye damage studies, and our work has shown that this is indeed the case.

Our work, which was performed during the years 1993-1996, was successfuly carried to completion and has resulted in several journal publications [1]-[9] and presentations at national and international meetings. Basically, the research performed is divided into three sections, namely

1. Fundamental issues concerning arrest of collapse in transparent media.
2. Development of reliable models for collapse and optical breakdown in transparent media, in particular water.
3. Nonlinear effects at highly absorbing interfaces.

In the following paragraphs we provide overviews of the work conducted with details given in the following Sections. Section (1) describes our fundamental studies of the arrest of collapse in transparent media displaying normal group-velocity dispersion (GVD). It had previously been suggested on the basis of numerical simulations that normal GVD can arrest the spatial collapse associated with the envelope equations by casuing pulse-splitting. To verify this conclusion we developed a theory of critical collapse for pulses in the presence of normal GVD [1]. However, further studies showed that normal GVD alone is not enough to arrest collapse [2], but rather the collapse occurs at higher peak powers as the GVD is increased, that is, it delays the collapse as oppossed to removing it completely.

Section (2) contains the bulk of the work conducted, and deals with the development of reliable models for ultrashort pulse propagtion in water as a model for propagation in the vitreaous humor. In particular, we have developed a comprehensive model for propagation in water which accounts for self-focusing collapse, normal GVD, multi-photon absorption and avalanche breakdown. This work was conducted in close collaboration with our colleagues at the Armstrong Laboratory, Brooks AFB, and resulted in the transfer of an operational code for nonlinear propagation in the vitreous humor which was later used for studies of eye damage. In particular, we maintained regular contact with Drs. Richard Albanese and Mary Potasek at the Mathematical Products Division and Drs. Mark E. Rogers, Pat Roach, Randy Thompson and Paul Kennedy at the Optical Radiation Division. This interaction was mediated in the form of regular contract reviews, meetings and Lab. visits which are tabulated in Sec. 5.

The final Section (3) deals with nonlinear effects at highly absorbing interfaces. This problem is relevent to the optical properties for light incident from the vitreous humor onto the retina, in particular the highly absorbing

retinal pigment epithelium in which damage can occur. At present very little is known about the nonlinear properties of highly absorbing interfaces but it is clear that the usual envelope equations must fail as the absortpion per wavelength approaches unity. We have investigated nonlinear refection properties in this regime and have discovered a new phenomenon, the Nonlinear Optical Skin Effect (NOSE) in which a short pulse reflected from the nonlinear absorber suffers a Doppler shift resulting from a moving boundary induced in the medium [8].

In the remaining Sections we now provide more details of each area of research.

1 Fundamental Issues

Our work has served to elucidate the understanding of self-focusing collapse of ultrashort pulses. In particular, we investigated the issue of whether normal GVD can halt self-focusing collapse as has been proposed, and also whether collpase is a feature of the full solution of Maxwell's equation. Highlights of this area include

- An analytic theory of the effects of normal GVD on collapse showing its arrest close to the critical power [1].
- Derivation of the threshold power for collapse in the presence of GVD [2].
- Numerical study of the conical emission and spectral broadening which accompany collapse and their roles as signatures of pulse-splitting [3].
- Development of a numerical scheme for soling the full Maxwell's equations for nonlinear optics.
- Theoretical prediction of carrier wave shocking for femtosecond optical pulses [4].

1.1 Arrest of crtitical collapse by GVD

To address the effects of normal GVD on SF collapse we generalize the usual steady-state SF equation to allow for pulsed operation. Then taking $A(x,y,t;z)$ to be the envelope of the singly polarized electric field $\vec{E}$ with carrier wave $\exp(ikz - i\omega t)$, $k = \frac{n(\omega)\omega}{c}$, and introducing the retarded time

$\hat{t} = t - k'z$, $k' = (\omega')^{-1}$ is the inverse group velocity of the wavepacket, we obtain the scaled propagation equation

$$A_z = i\nabla^2 A + i|A|^s A - i\gamma A_{tt}, \tag{1}$$

where we now understand t to represent the retarded time $t - k'z$. In (1), the transverse coordinates have been scaled with $\sqrt{2k}$, γ is $\frac{1}{2}k'' = -\frac{1}{2\omega'^3}\omega''$. We denote by d the number of transverse dimensions. Here $d = 1$ or 2. We take the order of nonlinearity s to be such that $sd = 4$ so that here $s = 4$ or 2. The case where $k'' > 0 (k'' < 0)$ is called normal (anomolous) dispersion. For pulses in the 100 femtosecond to 1 picosecond and beyond range with beam widths of the order of millimeters, dispersion along the pulse propagation direction is small when compared to diffraction. Therefore, at least initially, the term γA_{tt} is small and each individual cross-section of the pulse pursues its own dynamics independent of the others.

In the absence of GVD each time slice in the pulse is assumed to collapse in the self-similar form

$$A(\tau, \xi, t) = g^{\frac{d}{2}}\chi(\xi)\exp[-i\frac{\alpha\xi^2}{4} + i\tau], \tag{2}$$

after capturing a critical number of photons. The function $\chi(\xi)$ gives the shape of each cross-section, and the new independent variables are defined as

$$\xi = g\rho, \tag{3}$$

$$\tau = \int^z g^2 dz', \tag{4}$$

where $\alpha = g_\tau/g$, and the operators transform as $\partial_z = g^2(\alpha\xi\partial_\xi + \partial_\tau)$ and $\nabla_\rho^2 = g^2\nabla_\xi^2$. A special combination of g and its derivatives also arises in this analysis and is defined as,

$$\beta = \frac{1}{4}(\alpha_\tau + \alpha^2). \tag{5}$$

This new variable is proportional to the difference of the local curvature and twice the square of the local scale length of g.

In the absence of dispersion, the equations

$$\frac{dg}{d\tau} = \alpha g, \tag{6}$$

$$\frac{d\alpha}{d\tau} = 4\beta - \alpha^2, \tag{7}$$

$$\frac{d\beta}{d\tau} = -\alpha v(\beta), \tag{8}$$

describe the evolution of g, α, and β on the collapsing filament where $a = d\langle R_0^2\rangle/\langle\xi^2 R_0^2\rangle$ is the dimension times the photon number divided by the width of the ground state solitary wave of the cross section at $t = 0$.

To proceed we extend the above analysis of the self-similar collapse which has been so successful in the sign definite case to help us understand what the effect of normal dispersion is on the pulse as it begins to collapse in d-dimensions. First we are going to assume that (i) the strength of the term with positive dispersion, γ/t_o^2, where t_o is the initial pulse width, is small, and (ii) the central cross section of the pulse, which we take to be $t = 0$, has sufficient photons so that it collapses and reaches self-similar form (2).

Using the self-similar form of A, as stated in (2), the dispersion term is rewritten as,

$$\partial_t A = -\partial_t z_0 \partial_z A \,, \tag{9}$$

$$\partial_t^2 A = -\partial_t^2 z_0 \partial_z A + (\partial_t z_0)^2 \partial_z^2 A \,. \tag{10}$$

At the peak of the envelope (10) simplifies. First, $\partial_t z_0|_{t=0} = 0$ for a symmetric initial pulse centered at $t = 0$. Second, each of the neighboring cross-sections have longer collapse distances making $\partial_t^2 z_0|_{t=0} > 0$. Thus, in the neighborhood of $t = 0$ at which the first collapse occurs,

$$\partial_t^2 A = -\partial_t^2 z_0 \partial_z A \,, \tag{11}$$

and $i\gamma A_{tt} = \epsilon(1 - i\epsilon)^{-1}(\nabla^2 A + |A|^s A)$, where $\epsilon = \gamma z_0'' > 0$. The equation for A now reads,

$$A_z = i\nabla^2 A + i|A|^s A - \epsilon(1 - i\epsilon)^{-1}(\nabla^2 A + |A|^s A) \,. \tag{12}$$

Substituting the self-similar form (2) into (12), and using the new variables defined in (3) – (5), it is found that

$$i\ \partial_\tau \chi - \chi + \nabla_\xi^2 \chi + |\chi|^s \chi + \beta\xi^2 \chi = -\epsilon[\partial_\tau \chi + \alpha\xi\partial_\xi \chi + \frac{d\alpha}{2}\chi + i\chi - i(\beta + \frac{\alpha^2}{4})\xi^2 \chi] \,. \tag{13}$$

This equation gives the evolution of the transverse profile, χ, as long as α and β are known.

For our purposes we can obtain equations for α and β from the solvability condition of the first-order solution in the asymptotic expansion of χ, where

$$\chi = \chi_0 + \chi_1 + \chi_2 + \cdots \,, \tag{14}$$

and it is assumed that $\alpha^2 \gg \partial_\tau \alpha$, $\partial_\tau \chi \ll 1$, and $\beta \ll 1$ as $\tau \to \infty$. The zero-order equation in this expansion is

$$\nabla_\xi^2 \chi_0 - \chi_0 + |\chi_0|^s \chi_0 + \beta \xi^2 \chi_0 = 0 \ , \tag{15}$$

and its solution should satisfy the conditions $\chi(\infty) = \chi_\xi(0) = 0$. Near the peak for small $\beta\xi^2\chi_0$, (15) is approximated by the ground state stationary solution of the d-dimensional NLS with $\gamma = 0$ in (1), R_0.

The first-order equation is

$$\begin{aligned} L\chi_1 \ + \ & \frac{s}{2}|\chi_0|^{s-2}\chi_0^2\chi_1^* = -iv(\beta)\chi_0 - i\partial_\tau\chi_0 \\ - \ & \epsilon[\alpha(\frac{d}{2} + \xi\partial_\xi)\chi_0 + i\chi_0 - i(\beta + \frac{\alpha^2}{4})\xi^2\chi_0] \ , \end{aligned} \tag{16}$$

where

$$L = \left[\nabla_\xi^2 - 1 + \beta\xi^2 + (\frac{s}{2}+1)|\chi_0|^s\right] \ .$$

By rewriting (16) in terms of the real and imaginary parts of χ_1 using $\chi_1 = \delta + i\psi$, and $\partial_\tau\chi_0 = \partial_\beta\chi_0\partial_\tau\beta$ one obtains,

$$L_+\delta = -\epsilon\alpha(\frac{d\chi_0}{2} + \xi\partial_\xi\chi_0) \ , \tag{17}$$

$$L_-\psi = -\partial_\beta\chi_0\partial_\tau\beta - \epsilon[1 - (\beta + \frac{\alpha^2}{4})\xi^2]\chi_0 - v(\beta)\chi_0 \ , \tag{18}$$

where

$$L_\pm = \nabla_\xi^2 - 1 + \beta\xi^2 + (\frac{s}{2}+1)|\chi_0|^s \pm \frac{s}{2}|\chi_0|^{s-2}\chi_0^2 \ . \tag{19}$$

It has been assumed that $\xi \sim O(1)$ near $\rho = 0$ and that the term $\beta\xi^2\chi_1$ is small. The solvability condition for (18) requires that

$$\langle R_0|\partial_\beta\chi_0\rangle\partial_\tau\beta = -v(\beta)\chi_0 - \epsilon[\langle R_0^2\rangle - (\beta + \frac{\alpha^2}{4})\langle\xi^2 R_0^2\rangle] \ . \tag{20}$$

Using the relation, $\langle R_0|\partial_\beta\chi_0\rangle = \langle\xi^2 R_0^2\rangle/d$, the evolution of g is given by the set of ordinary differential equations

$$\frac{dg}{d\tau} = \alpha g \ , \tag{21}$$

$$\frac{d\alpha}{d\tau} = 4\beta - \alpha^2 \ , \tag{22}$$

$$\frac{d\beta}{d\tau} = -av(\beta) - \epsilon(a - \frac{\alpha^2}{4} - \beta) \ . \tag{23}$$

This reduced set of equations (21) – (23) describes the evolution of the parameters of the self-similar solution near the peak of the envelope in the presence of normal dispersion. As in the unperturbed case, the behavior of g indicates whether collapse occurs.

We now analyze the phase portrait of (22) and (23). In Fig. 1 the phase portrait of (22) and (23) is shown for $\epsilon = 0.1$, $s = 2$ and $d = 2$. In this case $a = 1.674$. For any finite value of the dispersion the point at $\alpha = \beta = 0$ is no longer an attracting limit point. Trajectories that would have collapsed for $\gamma = 0$ now tend to $\alpha < 0$. Since g is positive g_z must be negative and these trajectories must correspond to solutions that do not collapse, since $\alpha = g_\tau/g$. At $\alpha = 0$ the peak intensity of the pulse reaches its maximum and begins to decrease.

Note that this pair of equations has two fixed points which lie on the parabola $\beta = \alpha^2/4$. The right branch of this parabola has a hyperbolic fixed point while the left has a source. Above these points and to the right of the left branch of the parabola trajectories tend to infinity along $\beta = \alpha^2/4$. It is easy to show that these fixed points originate at infinity as ϵ is made finite. As ϵ is increased, this pair of points moves toward the origin approaching a point near $\beta = 2$ as ϵ tends to infinity. These fixed points are therefore not relevant to the behavior of the filaments because they are so far away from the trajectories along which the initial surge towards collapse occurs.

Also note that the number of negatively dispersive coordinates, d, enters into the first-order equation (16) through the linear operator on the left hand side and only in the second, almost purely real, term on the right hand side. Because of this, d, and thus s, only enter the reduced equations through ϵ and a and then only in (23). Since the structure of the phase portrait of the reduced equations is relatively insensitive to variations in ϵ and a we find the surprising result that in addition to being qualitatively similar, the evolution of wave packets of different dimension undergoing critical collapse when perturbed by normal dispersion is also quantitatively similar.

Thus we have shown analytically that a finite amount of dispersion has the effect of arresting the self-similar collapse of a pulse. We have also verified this conclusion using numerical simulations [1].

1.2 Threshold for collapse

Although normal GVD can arrest critical collapse, this is not the case if the input power is sufficiently large, or the GVD too small. To address this

question we return to the NLSE in dimensional form

$$2ik\left(\frac{\partial A}{\partial z}+\frac{\partial k}{\partial \omega}\frac{\partial A}{\partial t}\right)+\nabla_{\perp}^{2}A-k\frac{\partial^{2}k}{\partial \omega^{2}}\frac{\partial^{2}A}{\partial t^{2}}+2k^{2}\frac{n_{2}}{n_{0}}|A|^{2}A=0\ . \qquad (24)$$

We have conducted extensive numerical simulations of (24) with $n_2 > 0$, $\partial^2 k/\partial\omega^2 > 0$, and initial data of the form $A(x,y,z=0,t) = \exp(-(x^2+y^2)/2\mathrm{w}_0^2 - t^2/2t_p^2)$, to explore the dynamics of pulse propagation. These simulations have shown that as the input power is increased a threshold, P_{TH}, is reached where self focusing dominates the initial dynamical evolution of the pulse. Near P_{TH} the pulse splitting process coincides with the arrest of the collapse at the peak of a pulse.

The solutions of (24) are functions of only two parameters when Gaussian initial data is used. We have chosen to write the first parameter as $\gamma = L_{DF}/L_{DS}$, which measures the strength of the dispersion relative to diffraction, where $L_{DS} = t_p^2/k''$ is the linear dispersion length, and $L_{DF} = \mathrm{w}_0^2 k_L/2$ is the diffraction length. The second parameter, p, measures the strength of the nonlinearity and is the ratio of the peak input power, P, of a Gaussian pulse to the critical power for 2D self focusing, $P_c = (1.22)^2\pi\lambda^2/(32 n_0 n_2)$.

The self-focusing threshold in normally dispersive media is greater than that for stationary 2D self focusing so $P_{TH} > 1$. Below P_{TH}, pulse splitting may occur only after the pulse has passed its focus. For $P \geq P_{TH}$ pulse splitting occurs at or before the focus of the pulse. For a series of values of the dispersion parameter γ, we have numerically integrated (24) to determine the threshold power, P_{TH}. This threshold is plotted in Fig. 2, where the filled circles indicate simulations that were below the threshold, P_{TH}, and the open circles indicate simulations that were above.

An analytic estimate for the threshold power P_{TH} can be obtained using physical arguments. This estimate is based on the idea that when the length scale for self focusing is comparable to the length scale for which nonlinear dispersive spreading reduces the peak power below the 2D critical power, self focusing should be prevented. The self-focusing length scale, z_{SF}, corresponding to the peak input power in the absence of GVD ($\gamma = 0$) is

$$z_{SF}/L_{DF} = 0.367\left[(p^{\frac{1}{2}} - 0.852)^2 - 0.0219\right]^{-\frac{1}{2}}\ . \qquad (25)$$

This length scale is an improved version of that conjectured by Kelley on the premise that the collapse should occur near the focal point of the nonlinear

lens induced by the incident beam. The dispersion length scale, z_{NLGVD}, taking into account nonlinear effects, is that length over which the combined effects of self-phase modulation and normal GVD would reduce the peak power from its input value to the critical power $p = 1$ in the absence of diffraction. To obtain z_{NLGVD}, we use an approach previously developed by Potasek *et.al.* for pulse spreading in optical fibers. A temporal analogy of Kelley's approach to self focusing is employed whereby one considers the "temporal lens" induced by the incident (on-axis) pulse which frequency chirps the field. Normal GVD then causes the propagating pulse width $\sigma(z)$ to increase from its initial value $\sigma(0)$ according to

$$\frac{\sigma(z)}{\sigma(0)} \simeq \sqrt{1 + (\frac{\gamma}{\beta} + 2^{\frac{1}{2}})(4\gamma\beta(z/L_{DF})^2) + \left(\frac{16}{27}\right)^{\frac{1}{2}}(4\gamma\beta(z/L_{DF})^2)^2}\ . \quad (26)$$

In passing from the notation of Potasek et. al. to ours we have used $\phi_m = 2\beta z/L_{DF}$, $d_{eff} = 2\gamma z/L_{DF}$. Note that when $\beta = 0$ the variation of the pulse width is due only to linear spreading. When γ is small with respect to β the linear term may be ignored. By assuming that the propagating pulse remains roughly Gaussian so that $p(0)\sigma(0) = p(z)\sigma(z)$, and setting $p(0) = p$, and $p(z) = 1$, in (26), the dispersion length, z_{NLGVD}, can be written in terms of p and γ.

The dynamics of the pulse evolution are dictated by the relation between z_{SF} and z_{NLGVD}. For $z_{SF} > z_{NLGVD}$ we expect normal GVD to lower the peak power of the pulse enough to prevent collapse, so $p < P_{TH}$. In contrast, for $z_{SF} < z_{NLGVD}$ spatial self focusing should dominate the dynamics and will correspond to $p > P_{TH}$. An estimate for the threshold power P_{TH} in terms of the dispersion parameter γ can be obtained by letting $z_{SF} = z_{NLGVD}$. Excluding the linear contributions,

$$z_{NLGVD}/L_{DF} = \sqrt{\frac{\left[3.38 + 5.2(p^2 - 1)\right]^{\frac{1}{2}} - 1.84}{15\gamma p}}\ , \quad (27)$$

and,

$$\gamma \simeq \frac{\left\{\left[3.38 + 5.2(P_{TH}^2 - 1)\right]^{\frac{1}{2}} - 1.84\right\}\left[(P_{TH}^{\frac{1}{2}} - 0.852)^2 - 0.0219\right]}{2P_{TH}}\ . \quad (28)$$

This analytic estimate is displayed as the solid line in Fig.2. It provides an excellent characterization of the numerical data over a wide range of γ. It

works well for both $\gamma \ll 1$, which is the experimentally important parameter regime, and for $\gamma \sim 1$. If the linear spreading distance, z_{GVD}, is used, where $\beta = 0$ in (26), one obtains the curve annotated with dots and dashes, (-·-), plotted in Fig. 2.

1.3 Other issues

The main findings of this section are that normal GVD can arrest collapse for powers close to critical, but only for powers below a threshold value dependent upon the value of the GVD. Below this threshold the collapse is arrested via pulse-splitting, but above the threshold even the pulse splitting is not sufficient to arrest collapse before the envelope approximations fail.

In view of the importance of these results we have investgated the collaspe further to look for potential experimental signals of the pulse-splitting phenomenon [2]. Our numerical simulations show that conical emission accompanys pulse-splitting, the frequency of the emitted cone being dependent on the value of the GVD. The conical emission is also accompanied by significant superbroadening of the pulse, and is responsible for the pulse-splitting phenomenon. We have related both the spectral super broadening and conical emission to a fundamental four-wave interaction which can become phase-matched via the normal GVD.

We have also begun to explore the arrest of SF collapse beyond the envelope approximation. For this we have developed Maxwell equation solver which are capable of handling nonlinearity. Numerical simulations indicate that vectorial field effects arrest collapse as the field approaches wavelength scales, even in the absence of normal GVD. However, there is no supporting theory for this at present. We have also discovered a new phenomenon which is beyond the envelope approximation, namely, carrier wave shocking [4]. Optical shocks have been studied for sometime in the area of nonlinear fiber optics. These shocks appear, however, in the field envelope. We have found that for ultrahort pulses shocks can start to appear on the carrier, and is characterized by the appearence of a strong third-harmonic. Carrier shocks may play a significant role in the arrest of SF collapse when the pulse length contracts and the intensity gets very large, since the energy converted to the thrid-harmonic may be sufficient to reduce the fundamental power below critical.

2 Self-focusing and Optical Breakdown

In this section we describe our achievments in the area of modelling of SF and LIB in water as a model for the vitreous humor. The full details of our extensive numerical studies are presented in Refs. [5, 6], and here we display the most revealing results. Research highlights include

- Development of a comprehensive model for nonlinear propagtion including SF, GVD, LIB, and MPA [6].
- Development of a code for nonlinear propagation which was transferred to Brooks Air Force Base for studies of eye damage.
- Analytic criteria for the relative roles of SF and LIB as a function of pulse length and focusing conditions [5].
- Calculations of breakdown thresholds with and without SF and comparison with previous theories and experiments where possible. This provided validation of the model.
- Demonstration that SF and LIB are both key players in ultrashort pulse propagtion in water.
- Detailed investigation of strongly nonlinear behavior of ultrshort pulse collapse shwoing pulse splitting and potentially new mechanisms for eye damage.

2.1 Theoretical Model

To start we describe the general theoretical model for for nonlinear propagation in water which is a generalization of the model previously studied by Feit and Fleck [10] to include GVD, SF, and MPA. Then assuming propagation along the z-axis, the equation for the electric field envelope $\mathcal{E}(r,z,t)$ in a reference frame moving at the group velocity is

$$\frac{\partial \mathcal{E}}{\partial z} = \frac{i}{2k}\nabla_T^2\mathcal{E} - \frac{ik''}{2}\frac{\partial^2\mathcal{E}}{\partial t^2} + ik_0n_2|\mathcal{E}|^2\mathcal{E} - \frac{\sigma}{2}(1+i\omega\tau)\rho\mathcal{E} - \frac{\beta^{(K)}}{2}|\mathcal{E}|^{2K-2}\mathcal{E}, \quad (29)$$

where the terms on the right-hand-side describe transverse beam diffraction, GVD, nonlinear SF, absorption and defocusing due to the electron plasma, and MPA involving K photons, respectively. Here ω is the optical frequency, $|\mathcal{E}|^2$ the intensity, $k = n_b k_0 = n_b\omega/c$, the quantity $k'' = \partial^2 k/\partial\omega^2$ controls

the magnitude and sign of the GVD, with $k'' > 0$ corresponding to normal dispersion and $k'' < 0$ to anomolous dispersion, n_2 is the nonlinear coefficient such that the nonlinear change in refractive-index is $n_2|\mathcal{E}|^2$, σ the cross-section for electron-neutral inverse bremsstrahlung, τ is the electron collision relaxation time, and $\beta^{(K)}$ is the nonlinear coefficient for K-photon absorption. The order of the MPA is obtained from $K = mod(E_g/\hbar\omega) + 1$, which is the minimum number of photons of energy $\hbar\omega$ needed to overcome the ionization energy E_g for liberating an electron from a water molecule.

The Drude model equation which describes the electron density ρ is [11]

$$\frac{\partial \rho}{\partial t} = \frac{1}{n_b^2}\frac{\sigma}{E_g}\rho|\mathcal{E}|^2 + \frac{\beta^{(K)}|\mathcal{E}|^{2K}}{K\hbar\omega} - a\rho^2. \tag{30}$$

The first term on the right-hand-side of this equation describes growth of the electron plasma by cascade (avalanche) ionization, the second term is the contribution of MPA, which acts both as a source for the cascade process and as a contributor to plasma growth, and the third term describes the radiative electron recombination. In addition, if there is a free-electron density in the water prior to the pulse it will also be amplified by cascade ionization. Thus we also include a background initial density ρ_b as an initial condition for Eq. (30).

Fig. 3(a) shows the focusing geometry we considered. We are interested in the solutions of Eqs. (29) and (30) for an initial collimated Gaussian beam which enters the water sample following a lens of focal length f

$$\mathcal{E}(r,0,t) = \sqrt{\frac{2P_{in}}{\pi w_0^2}}\exp\left(-\frac{r^2}{w_0^2} - \frac{t^2}{t_p^2} - \frac{ikr^2}{2f}\right), \tag{31}$$

where P_{in} is the peak input power $[P(t) = \int 2\pi r dr\,|\mathcal{E}(r, z = 0, t)|^2 = P_{in}\exp(-2t^2/t_p^2)]$, w_0 the spot size, and $\tau_p = 2t_p$ is the full temporal width at the $1/e^2$ points of the pulse intensity distribution.

We have considered a specific focusing geometry with $f = 1.7$ cm, this being roughly the focal length of the eye. Unless otherwise stated the input spot size was taken as $w_0 = 200$ μm, which focuses at $d = 1.69$ cm with $w_f = 11.8$ μm. The Rayleigh range of the focused beam is $z_f = 0.1$ cm. The remaining parameters used for water for a wavelength of $\lambda_0 = 580$ nm are $n_b = 1.33$, $n_2 = 4.1 \times 10^{-16}$ cm^2/W, $K = 4$, $\beta^{(4)} = 1.55 \times 10^{-48}$ m^{5}W^{-3}, $E_g = 6.5$ eV, $\tau = 10^{-15}$ s, $K = 4$, $\sigma = 1.4 \times 10^{-17}$ cm^2, $k'' = 0.05$ ps^2/m, and $P_{cr} = 1MW$.

2.2 Light-induced breakdown with linear focusing

To provide a framework in which to view the numerical simulations with SF and LIB, we first looked at LIB with no SF. This is closely realized experimentally by the focusing geometry shown in Fig. 3(b). In the absence of SF we may simply solve Eq. (30) for the density at the linear focus of the beam

$$\rho(t) = \rho_{bg}(t) + \rho_{mp}(t), \tag{32}$$

where

$$\rho_{bg}(t) = \rho_b \varphi(t),\ \rho_{mp}(t) = \varphi(t)\frac{\beta^{(K)}}{K\hbar\omega}\int_{\infty}^{t}\frac{|\mathcal{E}(u)|^{2K}}{\varphi(u)}du,$$
$$\varphi(t) = \exp\left[\frac{\sigma}{n_b^2 E_g}\int_{\infty}^{t}|\mathcal{E}(u)|^{2K}du\right].$$

$\rho_{bg}(t)$ is the homogeneous part of the solution which arises from the background electron density ρ_b, and $\rho_{mp}(t)$ is the inhomogeneous solution which grows from the electron density initiated by MPA. Since the analytic solution (32) is not very informative, we have numerically solved the density equation (30) to obtain the threshold for LIB. Here we use as our criterion for LIB that $\rho(t = \infty) = \rho_{BD} \equiv 10^{18}$ cm^{-3}, where $\rho(t = \infty)$ is the final density following the pulse. This criterion for LIB was selected to coincide with the appearence of vapour bubbles in the water sample, also known as the bubble endpoint. The breakdown intensity versus pulse duration is shown in Fig. 4(a), and the breakdown power in Fig. 4(b), for the three backround densities $\rho_b = 0$ cm^{-3} (dotted line), 10^{10} cm^{-3} (solid line), and 10^{12} cm^{-3} (dashed line). The threshold intensity and power are seen to be insensitive to the background density for pulse durations less than 10 ps, and the variation in the predicted threshold is only a factor of two even for pulses as long as 200 ps.

Table I shows a comparison of the breakdown intensity I_{BD} calculated here (fourth column) with the previous experimental (second column) and first-order theoretical (third column) results of Kennedy et. al. [12, 13], and Hammer et. al. [14], with good overall agreement. The experiment of Hammer et. al. [14] was performed using a focusing geometry as in Fig. 3(b) with a thin water sample and at a wavelength of 580 nm. Comparison with the experimental data provides verification of the first-order model and also of the results from the Drude model contained in Eq. (30). This comparison gives validation of the Drude model as a reasonable model for ultrashort pulse LIB.

2.3 Multiphoton initiation versus background electron density

The calculations performed include components of the generated electron density which are initiated both from the background electron density ρ_b and from MPA. Both of these seed electron sources are amplified by cascade ionization. To determine which of these is the dominant seed electron source we have calculated the ratio of the background contribution to the total

$$\zeta = \frac{\rho_{bg}(\infty)}{\rho_{bg}(\infty) + \rho_{mp}(\infty)}. \tag{33}$$

By evaluating this ratio as a function of pulse duration we find that $\zeta = 1/2$ for $\tau_p = \tau_X = 160$ ps, so that MPA and the backround components are in exact balance. This value is further supported by the first-order model [12] which yields a pulse duration of $\tau_X = 120$ ps for the cross-over. For pulse durations less than the cross-over, $\tau_p < \tau_X$, MPA dominates the cascade initiation, and for $\tau_p > \tau_X$, the background density dominates the cascade initiation.

2.4 Numerical simulations with self-focusing

The simulations were performed using the beam propagation method in which the propagation is broken into small linear and nonlinear steps which are performed sequentially. Considerable advantage is gained by making use of the fact that for $P < P_{cr}$ or $P \sim P_{cr}$, in the initial stage of the propagation, when the nonlinear effect is not important and the plasma has not been generated, the propagation is described by the linear equation with only diffraction and dispersion. The solution of this equation can be written down exactly,

$$\mathcal{E}(r,t,z) = \mathcal{E}_0 D_f(r,z) D_s(t,z), \tag{34}$$

where

$$D_f(r,z) = \frac{1}{1+\frac{2iz}{k}\left(\frac{1}{w_0^2}+\frac{ik}{2f}\right)} \exp\left[\frac{-\frac{r^2}{w_0^2}-\frac{ikr^2}{2f}}{1+\frac{2iz}{k}\left(\frac{1}{w_0^2}+\frac{ik}{2f}\right)}\right],$$

$$D_s(t,z) = \frac{t_p}{\sqrt{t_p^2-2ik''z}} \exp\left(-\frac{t^2}{t_p^2-2ik''z}\right).$$

We use this linear equation to propagate the initial field into the nonlinear interaction zone, which is then used as the input to the nonlinear code. This

represents a considerable reduction in computation time, and also allows us to use the computational grid more effectively, since the bulk of the linear focusing by the lens is dealt with before passing over to the nonlinear propagation code.

Turning now to the numerical simulations with SF, we have determined the threshold for breakdown in the same manner as before. The results of our numerical simulations are summarized in Fig. 5 where we show (a) the breakdown threshold of peak input power (P_{in}), normalized to the critical power for collapse, and (b) the threshold intensity, both as functions of pulse duration τ_p. The solid circles in Fig. 5(a) are our data points corresponding to a peak plasma density of 10^{18} cm^{-3}. The solid curve is the threshold power curve obtained in the previous Section without SF, and also shown in Fig. 4(b). We see, therefore, that for pulses longer than $\tau_p = 10$ ps, the thresholds with and without SF agree very well. This is to be expected since for these pulse durations the breakdown power is considerably below the critical power, $P_{BD} < P_{cr}$, and SF plays only a minor role. In contrast, for $\tau_p < 10$ ps the breakdown power is seen to tend towards the critical power P_{cr}. This is to be expected intuitively, since as the input power approaches the critical power small changes in the input power can cause massive changes in the peak intensity at the laser beam focus, which in turn can cause very large changes in the peak plasma density generated, so that the plasma density for breakdown is easily reached. This is particularly true of the component of the density initiated by MPA since the source term varies as $|\mathcal{E}|^{2K}$ (see Eq. (30)), with $K = 4$, and MPA is expected to be the dominant initiation mechanism for plasma generation for pulse durations less than $\tau_X = 160$ ps.

The corresponding breakdown intensities, chosen as the peak intensities which appeared during the respective numerical simulations, versus pulse duration are shown in Fig. 5(b) (solid circles) along with the result without SF from Fig. 4(a) (solid line). Here we see a remarkable agreement, especially for longer pulses, between the results with and without SF. This agreement stems from the fact that LIB is triggered by the local electric field strength, or intensity, so that LIB has an intensity threshold [11] which is essentially independent of the focusing conditions.

Plasma shielding arises when the incident pulse energy is absorbed and converted to the generation of the electron plasma via LIB, thus shielding the region beyond the plasma from the full pulse energy. In Fig. 6 we show the peak generated plasma density and corresponding percentage energy absorbed for pulse durations $\tau_p = 200$ ps (solid line), 100 ps (dotted line),

and 20 ps (dashed line). In each case the lowest power indicated is slightly above the threshold power for LIB, with weak plasma shielding in each case. However, far above the threshold the peak plasma density and the plasma shielding both increase, with 10-25 % absorption depending on the pulse length. This clearly demonstrates that plasma shielding becomes more significant above the bubble endpoint threshold, as expected on physical grounds.

An interesting aspect of our model is the behavior of nonlinear propagation. Before the high-density plasma is generated, the propagation is essentially described by the self-focusing solution However, once the plasma it acts to absorb energy and defocus the beam. The process of absorption and defocusing could result in very rich nonlinear phenomena which have not been studied in detail. Here we report a case of numerical simulation that shows qualitatively different behavior from what we have described in the previous section. We chose a smaller input spot size, $w_0 = 120$ μm, so as to reduce the effect of linear focusing. This allows us to follow the nonlinear self-focusing, which is very explosive, within the limit of our code. The process of pulse propagation and plasma generation is presented in Figs. 7 and 8. Fig. 7 shows $max_t|e(r=0,z,t)/e_0|$ (top), $max_t\rho(r=0,z,t)$ (middle) and energy (bottom) as functions of propagation distance z. It is interesting to note that there are two peaks in $max_t\rho(r=0,z,t)$, one in front of and the other behind the focal point $z=f$. The spatial extension of the plasma generated is wider than all the cases described in previous sections. One can clearly see that the energy absorption occurs in a region where the plasma is generated, while in other regions of low plasma density, the energy is almost constant. Fig. 8 shows ρ (top) and e (bottom) as functions of (x,t) at three propagation distances: (a) $z=1.6869$, (b) $z=1.70043$, and (c) $z=1.73562$. The pulse starts to split in front of the focal point. While the trailing split piece (the shorter piece corresponding to higher plasma density) is damped once the splitting occurs, the leading piece continues to focus and generates high plasma density *behind* the focal point [see Fig. 8(c)]. Although here the energy absorption is relatively higher, the propagating pulse shows a tendency of not being absorbed. This suggests a possible damaging mechanism: The leading split piece of the pulse may escape the plasma generated in front of the focal point and reach the retina, causing additional damage.

3 Nonlinear Absorbing Interface

This section describes our work on nonlinear absorbing interfaces as a start to addressing the issue of nonlinear effects at the boundary between the transparent vitreous humor and the highly absorbing retinal pigment epithelium. The models investigated are not directly relevant to the eye but shine a great deal of light on the issues which arise at highly absorbing interfaces when the absorption per wavelength approaches unity. The key point is that in this regime the envelope approximation is invalid and an approach based on Maxwell's equations must be employed. Previous work in this area concentrated only on the steady-state properties whereas our interest was in ultrshort pulses. Research highlights include

- Theoretical prediction of a new effect whereby an incident pulse is Doppler-shifted as a result of reflection of a moving absorption front [8]
- Demonstration of induced focsuing of an ultrashort pulse reflected of a saturable absorber [9].

Here we concentrate solely on the new results on the nonlinear skin effect.

3.1 Nonlinear skin effect

In the linear optical skin effect a pulse incident from air is reflected from a highly absorbing interface after penetrating only a fraction of a wavelength into the absorbing medium, this distance being the skin depth The skin effect is therefore of fundamental importance in understanding the electrodynamics of pulse propagation at condensed matter interfaces. In addition, it belongs to an important class of optical problems for which the notion of an electromagnetic field envelope varying slowly on the scale of a wavelength simply does not apply.

We have discovered a nonlinear generalization of the skin effect. Broadly speaking, saturation of the absorption allows the incident field to penetrate beyond the linear skin depth into the medium, and this causes an absorption front to propagate into the medium which separates the regions of low (saturated) and high (unsaturated) absorption. The front is excited by the incident pulse which is in turn reflected from the sharp absorption front, yielding a self-reflected pulse. Thus the absorption front acts as a moving

mirror from which the pulse is self-reflected, and the pulse suffers a red-shift due to the Doppler effect.

We consider the time-dependent propagation of a linearly polarized plane electromagnetic wave incident on a nonlinear medium composed of two-level systems. For propagation along the z-axis, and taking the electric field polarized along the x-axis, Maxwell's curl equations take the form

$$\frac{\partial B_y}{\partial t} = -\frac{\partial E_x}{\partial z}, \qquad \frac{\partial D_x}{\partial t} = -\frac{\partial H_y}{\partial z}, \tag{35}$$

where $B_y = \mu_0 H_y$. The specification of the problem is completed with the constitutive relation $D_x = \epsilon_0 E_x + P_x$, where P_x is the optical polarisation. To elucidate the basic physics we employ a two-level model to describe the optical response with lower electronic state $|1\rangle$ and upper state $|2\rangle$. The Bloch equations are then

$$\frac{\partial \rho_{21}}{\partial t} + (\gamma_2 + i\omega_{21})\rho_{21} = i\frac{pE}{\hbar}n, \qquad \frac{\partial n}{\partial t} + \gamma_1(n-1) = 2i\frac{pE}{\hbar}(\rho_{21} - \rho_{21}^*), \tag{36}$$

where, ρ_{21} is the off-diagonal density matrix element, $n = (\rho_{11} - \rho_{22})$ is the population difference between the lower and upper states, ω_{21} is the transition frequency, p is the dipole moment in the field direction, and γ_1 and γ_2 are phenomenological damping constants for the population and polarisation, respectively. The polarization due to the atoms is then given by $P_x = N(z)p(\rho_{21} + c.c.)$, with $N(z)$ the density of two-level systems which varies along z in general.

We have solved the coupled Maxwell-Bloch Eqs. (35) and (36) using a standard discretization of the Maxwell equations as described by. The Bloch equations were integrated in time using a standard, fourth-order Runge-Kutta method. The system of equations was solved with the initial condition on the field

$$E_x(z, t=0) = E_0 \cos(2\pi\omega(z - z_0)/c) e^{-(z-z_0)^2/(ct_0)^2}, \tag{37}$$

along with a similar expression for B_y with $B_0 = E_0/c$. Here E_0 is the peak input electric field, $\omega = 2\pi c/\lambda_0$ is the central pulse frequency, $\tau_0 = 2t_0$ is the full-width at the $1/e^2$ points of the pulse intensity profile in time units, and z_0 is the position of the pulse center at $t = 0$. The nonlinear interface was imposed by tailoring the density profile $N(z) = \theta(z - z_{int})N_0$, with z_{int} the longitudinal position of the interface. The medium was initialized using $\rho_{21} = 0$, and $n = 1$ in the medium. When initializing the field we ensured that the field protruded negligibly into the nonlinear medium at $t = 0$.

In the limit of cw fields, as previously studied by Roso-Franco, the self-reflected wave arises when the normalized parameters,

$$\psi = \frac{p^2 N}{\epsilon_0 \hbar \gamma_2}, \qquad F = \frac{pE_0}{\hbar(\gamma_1\gamma_2)^{1/2}}, \tag{38}$$

are both greater than unity. Physically, ψ determines the linear absorption per wavelength, $\alpha\lambda_0 = 2\pi\psi$, and this quantity should be greater than unity for the linear skin effect. For saturation of the absorption and self-reflection $F > 1$ is required, since F^2 is the peak incident field intensity normalized to the cw saturation intensity.

We consider the transient regime in which the incident pulse width t_0 is much shorter than the population relaxation time $T_1 = \gamma_1^{-1}$, but longer than the polarization dephasing time $T_2 = \gamma_2^{-1}$, $T_1 >> t_0 > T_2$. For concreteness we adopt the following specific parameters, $\omega = \omega_{12} = 2 \times 10^{15}$ rads^{-1}, $t_0 = 300$ fs, $T_1 = 0.5$ ns, $T_2 = 50$ fs, $p = 5ea_0 = 4 \times 10^{-29}$ Cm, $N_0 = 4 \times 10^{19}$ cm^{-3} and $z_0 = -225$ μm. For these parameters $\psi = 3.8$ so that the linear skin effect is expected at low input intensities. We have numerically verified that this is indeed the case, and the input pulse suffers minimal distortion in profile or spectrum upon reflection.

Figures 9(a) and 1(b) show an example of the calculated pulses at two different times for a peak input field of $E_0 = 1.6 \times 10^8$ V/m. Although our calculations employ the full field, we display only the envelope obtained from joining the peaks as shown by the solid line, since it is not possible to resolve the carrier in the plots. The field strength is associated with the scale shown on the left-hand-side of the plots. In Fig. 9(a) for t=1.68 ps the peak of the input pulse has not yet reached the interface at $z_{int} = 400$ μm, but one can clearly see the leading edge of the pulse is penetrating only a short distance into the interface, as expected for the skin effect. The dashed line in Fig. 9(a), which is associated with the right-hand scale, is the local wavelength for the field. This is determined numerically by calculating the local wavenumber K via $K^2 \approx -E_x''/E_x$, where a prime signifies a z-derivative, and converting to wavelength. In Fig. 9(a) the local wavelength remains constant at the input value $\lambda_0 = 942$ nm. In contrast, Fig. 9(b) shows the field profile at a later time $t = 2.75$ ps following reflection from the interface (for times between the results shown in Figs. 9(a) and 9(b), the field profile shows strong ringing due to interference between the incident and reflected fields). The reflected pulse has developed a double-peaked structure (solid line), and become significantly chirped (dashed line). In particular, the central portion of the pulse has a peak local wavelength of 990 nm,

a significant red-shift. This red-shift is also evident in the reflected pulse spectrum (solid line) shown in Fig. 9(c) corresponding to Fig. 9(b), along with considerable spectral broadening and modulation (the input spectrum is shown by the dashed line and is associated with the left-hand scale).

The results shown in Fig. 9 are typical of what we observe in our simulations in the nonlinear regime, namely, distortion of the reflected field profile and significant spectral modulation and associated red-shift. To expose the physics underlying these phenomena we show in Fig. 10(a) and 10(b) the spatial distribution of the full field and the population difference $n = (\rho_{22} - \rho_{11})$ at various times corresponding to the results shown in Fig. 9. Figure 10(a) shows that the field penetrates progressively further into the interface as the absorption is saturated, as can be seen by comparing the field profiles at $t = 1.61$ ps (solid line) and $t = 1.95$ ps (dashed line) or $t = 2.28$ ps (single-dash-dot line) (at $t = 2.62$ ps the field has been mostly refelcted). At $t = 1.61$ ps (solid line) Fig. 10(b) shows that $n = 0$ before the interface signifying zero absorption, and $n = 1$ beyond the interface signifying large absorption due to the two-level systems. At later times after the input pulse has penetrated into the interface, the population difference is depleted and the absorption front is seen to propagate into the nonlinear medium. The propagating absorption front maintains a sharp wavelength scale transition region so that the linear skin effect still occurs but now from a moving absorption front. Thus the self-reflected field must suffer a red-shift due to the Doppler-effect, akin to reflection from a mirror moving away from a source. To validate this physical picture we have determined the absorption front velocity from the numerical simulation in Fig. 10(b), and the result is shown in Fig. 10(c). After initially accelerating the front reaches a maximum velocity of $v_{max}/c = 0.023$ before decelerating back to zero velocity. The maximum wavelength shift of the reflected pulse due to the Doppler effect is then $\Delta\lambda/\lambda_0 = 2v_{max}/c$ for $v_{max}/c \ll 1$ or $\Delta\lambda = 43$ nm for the free-space wavelength $\lambda_0 = 942$ nm used here. Thus, based on the Doppler effect we expect a maximum local wavelength of $\lambda = 985$ nm, in good agreement with the numerical results in Fig. 10(b). The Doppler effect upon reflection from the moving absorption front can therefore explain the magnitude of the observed pulse wavelength chirp.

To summarize, we have introduced the dynamic nonlinear optical skin effect for reflection of pulses from a highly absorbing interface. This new basic effect for the electrodynamics of interfaces combines the concepts of self-reflected waves and front propagation, and is also a prime example of a nonlinear optical phenomenon where the SVEA fails and the full Maxwell

equations must be employed. We have shown that the nonlinear optical skin effect arises from moving absorption fronts so that the red-shifting and spectral modulation of the reflected pulse are clear experimental signatures of the effect.

4 Personnel Supported

Faculty
A.C. Newell (PI)
J.V. Moloney
E.M. Wright
V.E. Zakharov

Postdoctoral Fellows

Q. Feng (50 %)
R. Flesch (50 %)
W. Forysiak (50 %)

Students

Kirk Cook

5 Interactions/Presentations

5.1 Participation/Presentations

- "Nonlinear Mechanisms for Laser Induced Breakdown of Femtosecond Pulses", 3rd AFOSR Ultrashort Laser Program Collaborative Workshop, Brooks Air Force Base, San Antonio, Texas. 14-16 December 1994.
- "Issues Relating to the Arrest of Critical Collapse of Femtosecond Pulses in Normally Dispersive Self-Focusing Media", invited talk - Conference on Nonlinear Coherent Structures in Physics and Biology, 10-14 July 1995, Heriot-Watt University Edinburgh.

- "Arrest of Critical Collapse of Ultra-Short Pulses in Optically Transparent Media", Physics Colloquium, Georgia Tech., 24 April 1995.
- "Issues in the Arrest of Critical Collapse of Femtosecond Optical Pulses in Optically Transparent Media", Physics Colloquium, Free University, Amsterdam, 28 June 1995.
- "Computational Nonlinear Optics", Computational and Physical Mathematics Contractors Meeting, Phillips Laboartory, Kirtland AFB, 28-30 June 1995.

5.2 Consultative and Advisory Functions to Other Laboratories and Agencies

- Visit by J. Moloney (UA) to "3rd AFOSR Ultrashort Laser Program Collaboartive Workshop", Brooks Air Force Base, San Antonio, Texas, 14-16 December 1994, to consult with Dr R. Albanese (AL/OES), Dr M. Potasek (AL/OES), Dr M. Rogers (AL/CA), Dr B. Rockwell (AL/OEOP), Dr P. Kennedy (AL/OEOP), Dr C. Cain (AL/OEOP) and Dr R Thomson (OpTech).
- Brooks Air Force visit to ACMS, Department of Mathematics, University of Arizona, 9-12 May 1995. Personnel involved included: J. Moloney (UA), E. Wright (UA), Q. Feng (UA), R. Thompson (Op Tech), P. Kennedy (AL/OEO) and M. Potasek (AL/OES).
- Brooks Air Force visit to ACMS, Department of Mathematics, University of Arizona. 17-20 August 1995. Discussion on modeling nonlinear propagation of picosecond and femtosecond laser pulses in water and in the eye. Personnel involved included: J. Moloney (UA), E. Wright (UA), Q. Feng (UA), R. Thompson (Op Tech), P. Kennedy (AL/OEO) and M. Potasek (AL/OES).
- Hosting and organisation of the AFOSR/ACMS "Nonlinear Optics" Workshop, Tucson, Arizona. 9-11 October 1995.

  This workshop acts a a contract review for AFOSR and brings Air Force Laboartory scienctists in direct contact with academic researchers.
- Deliverable: Computer Code to simulate critical self-focusing of picosecond pulses in ocular and related media with plasma generation

through avalanche ionization included. Code is currently being run by Dr Randy Thompson (Op Tech) and Dr Paul Kennedy (AL/OEO) at the Armstrong Laboratory.

References

[1] G. G. Luther, A. C. Newell, and J. V. Moloney, "The effect of normal dispersion on collapse events," *Physica D* **74**, 59-73 (1994).

[2] G. G. Luther, J. V. Moloney, A. C. Newell, and E. M. Wright, "Self-focusing threshold in normally dispersive media," *Opt. Lett.* **19**, 862 (1994).

[3] G. G. Luther, A. C. Newell, and J. V. Moloney, and E. M. Wright, "Short-pulse conical emission and spectral broadening in normally dispersive media," *Opt. Lett.* **19**, 789 (1994).

[4] R. G. Flesch, A. Pushkarev, and J. V. Moloney, *Phys. Rev. Lett.* **76**, 2488 (1996).

[5] Q. Feng, J. V. Moloney, A. C. Newell, and E. M. Wright, "Laser-induced breakdown versus self-focusing for focused picosecond pulses in water," *Opt. Lett.* **20**, 1958 (1995).

[6] Q. Feng, J. V. Moloney, A. C. Newell, E. M. Wright, K. Cook, P. K. Kennedy, D. X. Hammer, B. A. Rockwell, and C. R. Thompson, "Theory and simulation on the threshold of water breakdown induced by focused ultrashort laser pulses," *IEEE J. Quant. Electron.* **QE-33**, 127 (1997).27 (1997).

[7] J. A. Powell, E. M. Wright, and J. V. Moloney, "Reflection of localized beams from a nonlinear absorbing interface," *SIAM J. Appl. Math.* **54**, 774 (1994).

[8] W. Forysiak, R. G. Flesch, J. V. Moloney, and E. M. Wright, "Doppler shift of self-reflected optical pulses at an interface: Dynamic nonlinear optical skin effect," *Phys. Rev. Lett.* **76**, 3695 (1996).

[9] W. Forysiak, J. V. Moloney, and E. M. Wright, "Nonlinear focusing of femtosecond pulses as a result of self-reflection from a saturable absorber," *Opt. Lett.* **22**, 239 (1997).

[10] M. D. Feit and J. A. Fleck, Jr., "Effect of refraction on spot-size dependence of laser-induced breakdown," *Appl. Phys. Lett.* **24**, 169-172 (1974).

[11] E. Yablonovitch and N. Bloembergen, "Avalanche ionization and the limiting diameter of filaments induced by light pulses in transparent media," *Phys. Rev. Lett.* **29**, 907-910 (1972).

[12] P. K. Kennedy, "A first-order model for computation of laser-induced breakdown thresholds in ocular and aqueous media: Part I-Theory," *IEEE J. Quant. Electron.* **31**, 2241-2249 (1995).

[13] P. K. Kennedy, S. A. Boppart, D. X. Hammer, B. A. Rockwell, G. D. Noojin, and W. P. Roach, "A first-order model for computation of laser-induced breakdown thresholds in ocular and aqueous media: Part II-Comparison to experiment," *IEEE J. Quant. Electron.* **31**, 2250-2257 (1995).

[14] D. X. Hammer, R. J. Thomas, G. D. Noojin, B. A. Rockwell, P. K. Kennedy, and W. P. Roach, "Experimental investigation of ultrashort pulse laser-induced breakdown thresholds in aqueous media," to be published in *IEEE J. Quant. Electron.*, April 1996.

Table I: Breakdown threshold intensities (W/cm^2).

τ_p	Experiment[1]	First-order[2]	I_{BD}[3]
2.4 ps	5×10^{11}	6.66×10^{11}	8.6×10^{11}
400 fs	1.26×10^{12}	2.56×10^{12}	2.7×10^{12}
100 fs	5.6×10^{12}	5.46×10^{12}	5.4×10^{12}

1. Experimental thresholds for 50% probability of breakdown
2. First-order calculation of the intensity breakdown threshold.
3. Intensity breakdown threshold from present work.

FIGURE CAPTIONS

Fig. 1 The phase portrait of the reduced equations (22) and (23) for $s = 2$ and $d = 2$, where $a = 1.674$ and $\epsilon = 0.1$. The attracting point at $(\alpha, \beta) = (0, 0)$ is removed for finite ϵ. Trajectories tend to $\alpha < 0$ where no collapse takes place.

Fig. 2 Results of numerical simulations: The full (open) circles correspond to those simulations below (above) P_{TH}. The solid line displays the analytic estimate (28) for P_{TH} as a function the dispersion parameter γ. The line, (–··–), displays the estimate using linear spreading, and the dotted line using 5 times the linear estimate.

Fig. 3 Focusing geometries considered in the text: (a) The incident laser pulse is focused from air through a lens with $f = 1.7$ cm directly into a water sample, where it comes to a linear focus at $d = 1.69$ cm, and (b) the incident laser pulse is focused from air through a lens with $f = 1.7$ cm, back into air and onto a thin water sample at the linear focus.

Fig. 4 (a) The breakdown intensity I_{BD} versus pulse duration, and (b) the breakdown input power P_{BD} normalized to the critical power for collapse, $P_{cr} = 1$ MW. The three curves correspond to initial background densities of $\rho_b = 0$ (dotted line), $\rho_b = 10^{10}$ cm^{-3} (solid line), and $\rho_b = 10^{12}$ cm^{-3} (dashed line).

Fig. 5 LIB thresholds with SF: (a) Threshold power normalized to the critical power for collapse, and (b) the threshold intensity, both as a function of pulse duration τ_p. In (a) the solid circles give the threshold for a peak density of 10^{18} cm^{-3}, the triangles are the threshold powers obtained using the criterion of a peak density of 10^{19} cm^{-3}, the numbers above the triangles are the % absorption of energy from the pulse using this density, and the solid curve is the threshold power curve obtained without SF, as in Fig. 2(b).

Fig. 6 Peak plasma density (in units of 10^{18} cm^{-3}) and percentage of energy absorption as functions of input power for $\tau_p = 200$ ps (solid line), 100 ps (dotted) and 20 ps (dashed), with $\rho_b = 10^{10}$ cm^{-3}.

Fig. 7 On-axis maximum field $\max_t |e(r = 0, z, t)|$ (top), plasma density $\max_t \rho(r = 0, z, t)$ (middle) and total pulse energy (bottom, in arbitratry units) as functions of propagation distance z for $\tau_p = 200$ fs, $w_0 = 120$ μm and $P = 1.08 P_{cr}$.

Fig. 8 Surface plots of $|\mathcal{E}(x,0,z,t)|$ (bottom) and $\rho(x,0,z,t)$ (top) at three propagation distances: (a) $z = 1.687cm$, (b) $z = 1.7cm$ and (c) $z = 1.736cm$.

Fig. 9 Calculated field profiles (solid lines) for $E_0 = 1.6 \times 10^8$ V/m and (a) t=1.68 ps before the field enters the interface at $z_0 = 400$ μm, and (b) t=2.75 ps following reflection from the interface. In plots (a) and (b) we show only the envelope obtained from joining the field peaks. The field strength is associated with the left-hand scale and is normalized to unity. The dashed lines in (a) and (b) show the corresponding local wavelength over the pulse, and are associated with the right-hand scale. Fig. 1 (c) shows the corresponding pulse spectra. The input spectrum is shown dashed and is associated with the left-hand scale.

Fig. 10 Spatial distribution of a) the full field in the vicinity of the interface at $z_0 = 400$ μm, and b) the population difference n at times t = 1.61 ps (solid line), 1.95 ps (dashed line), 2.28 ps (single-dot-dashed line), and 2.62 ps (triple-dot-dashed line), where the front propagates to the right with increasing time, and c) the numerically calculated absorption front velocity normalized to c.

Figure 1

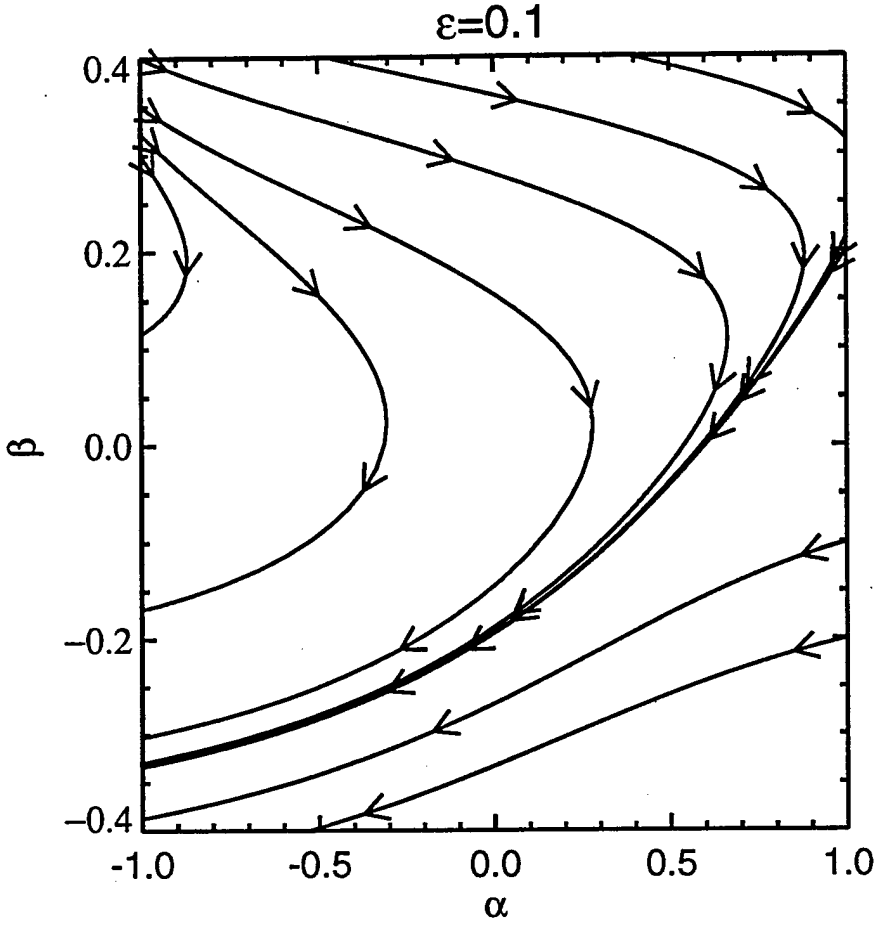

Figure 2

Map of Self Focusing in Normally Dispersive Media

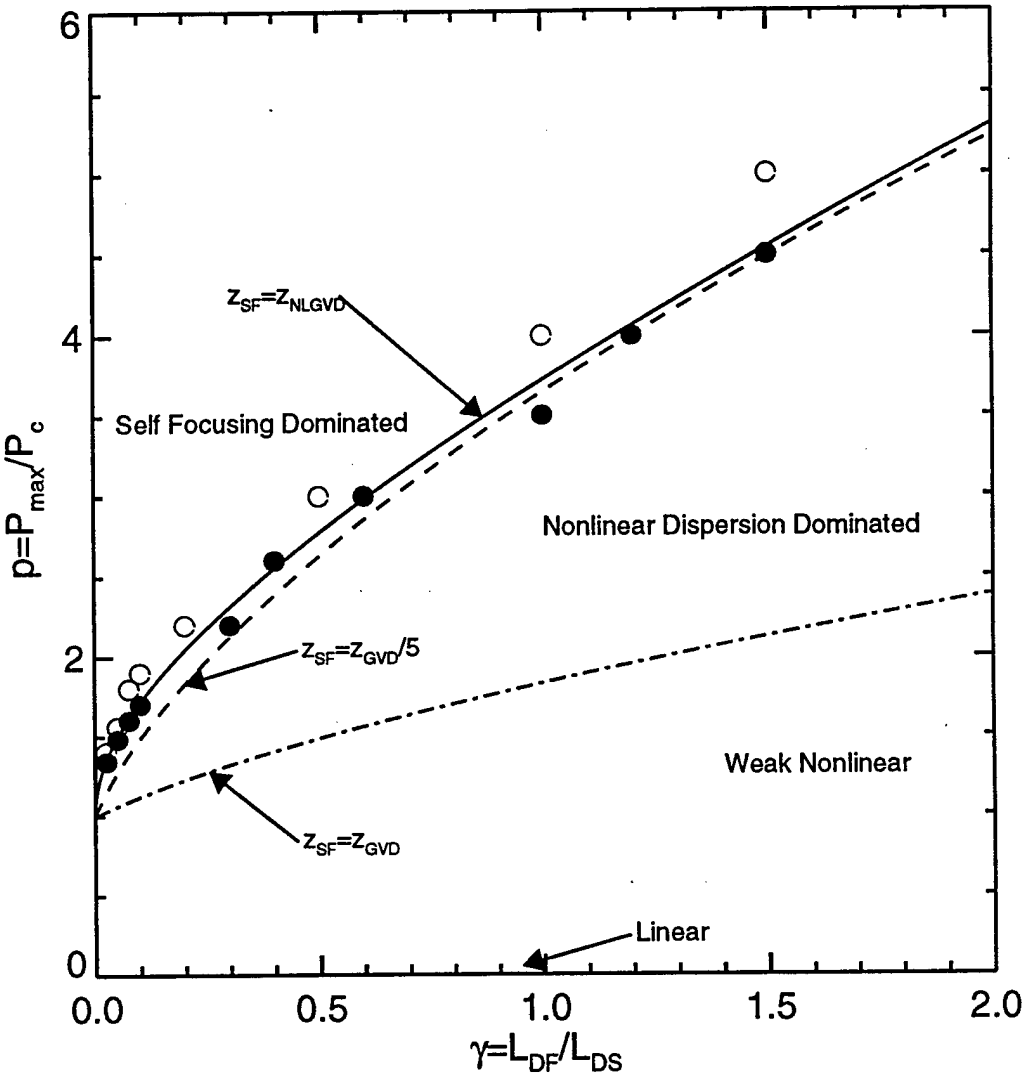

Figure 3

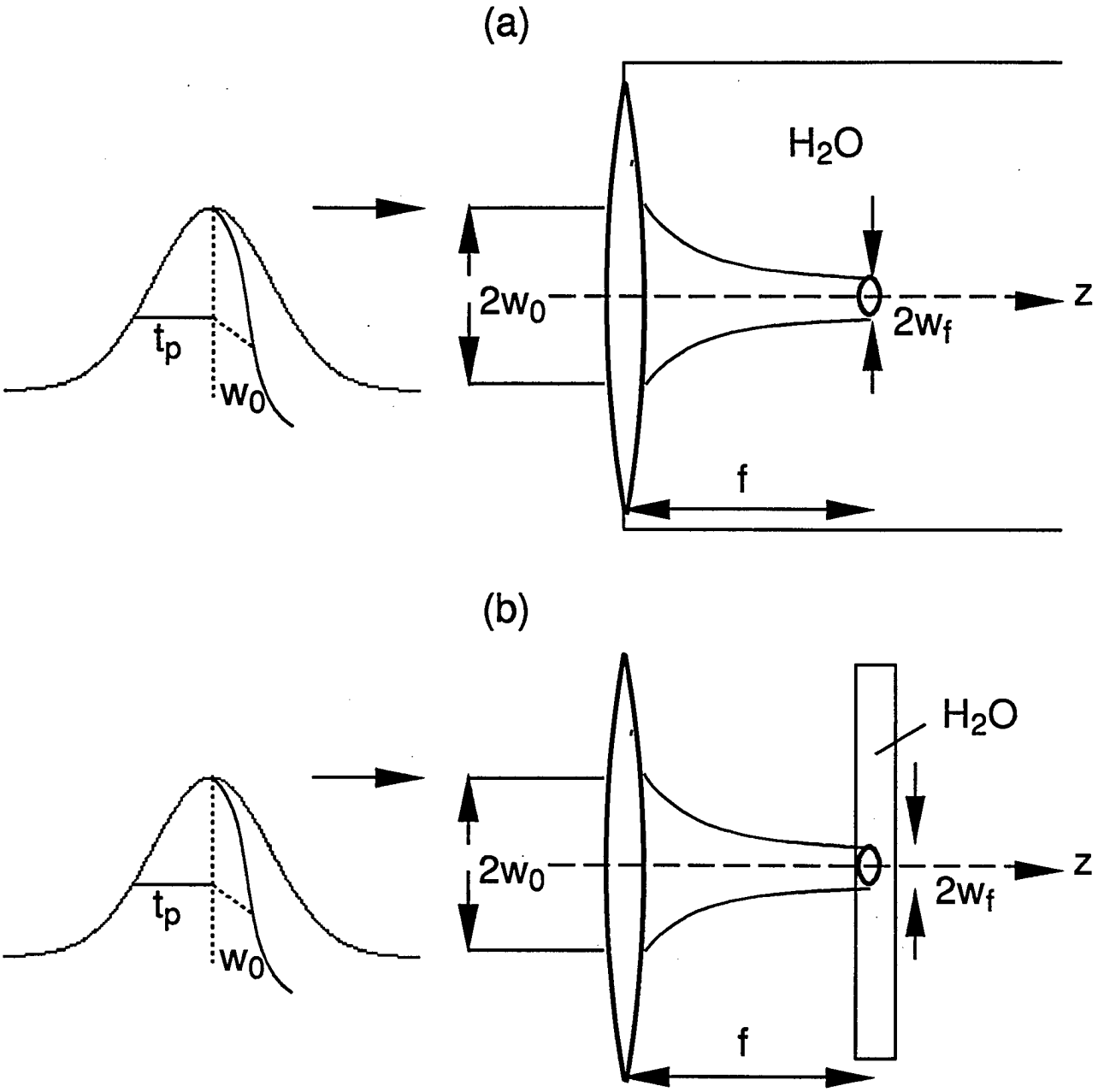

Figure 4

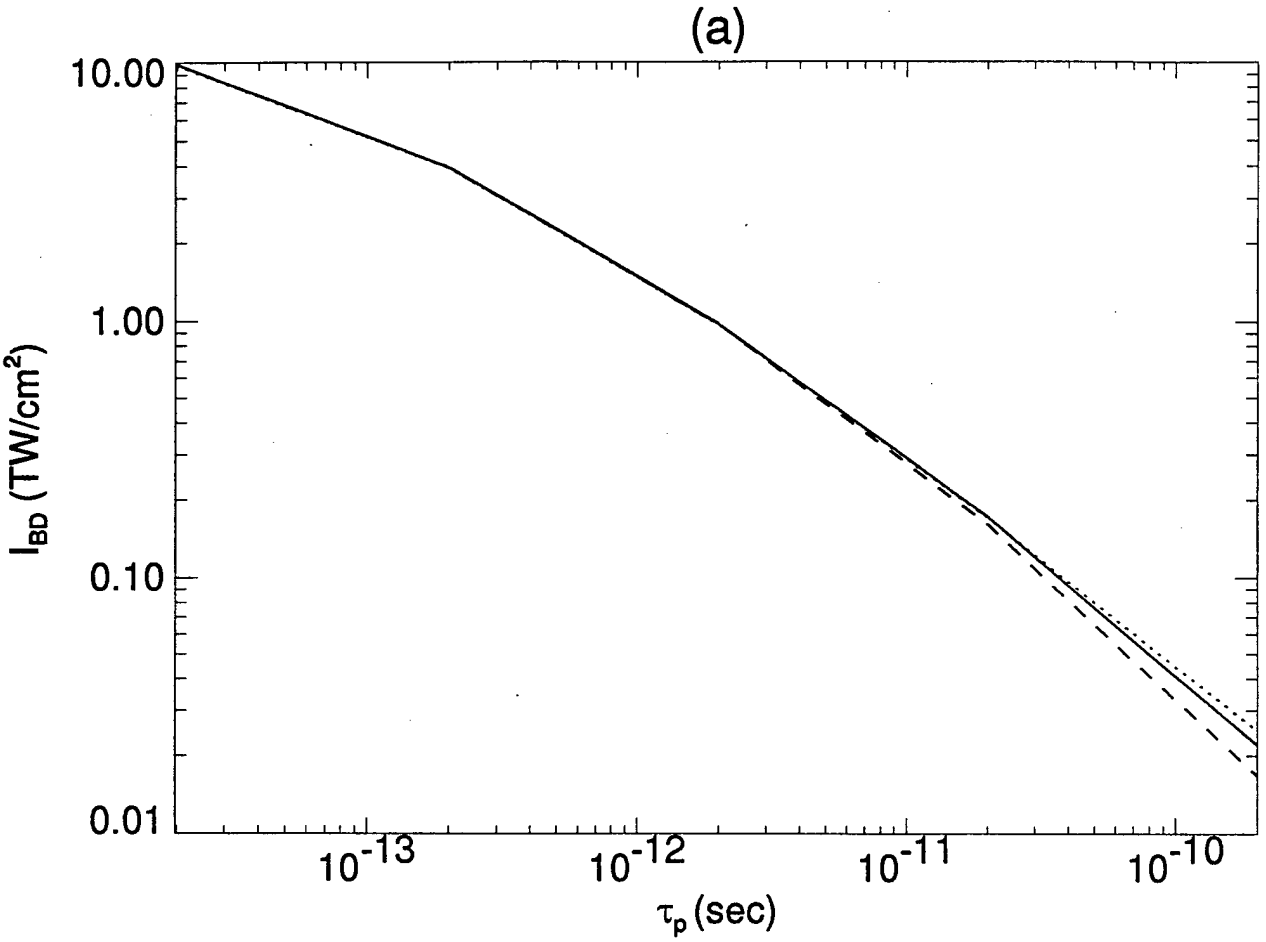

Figure 4

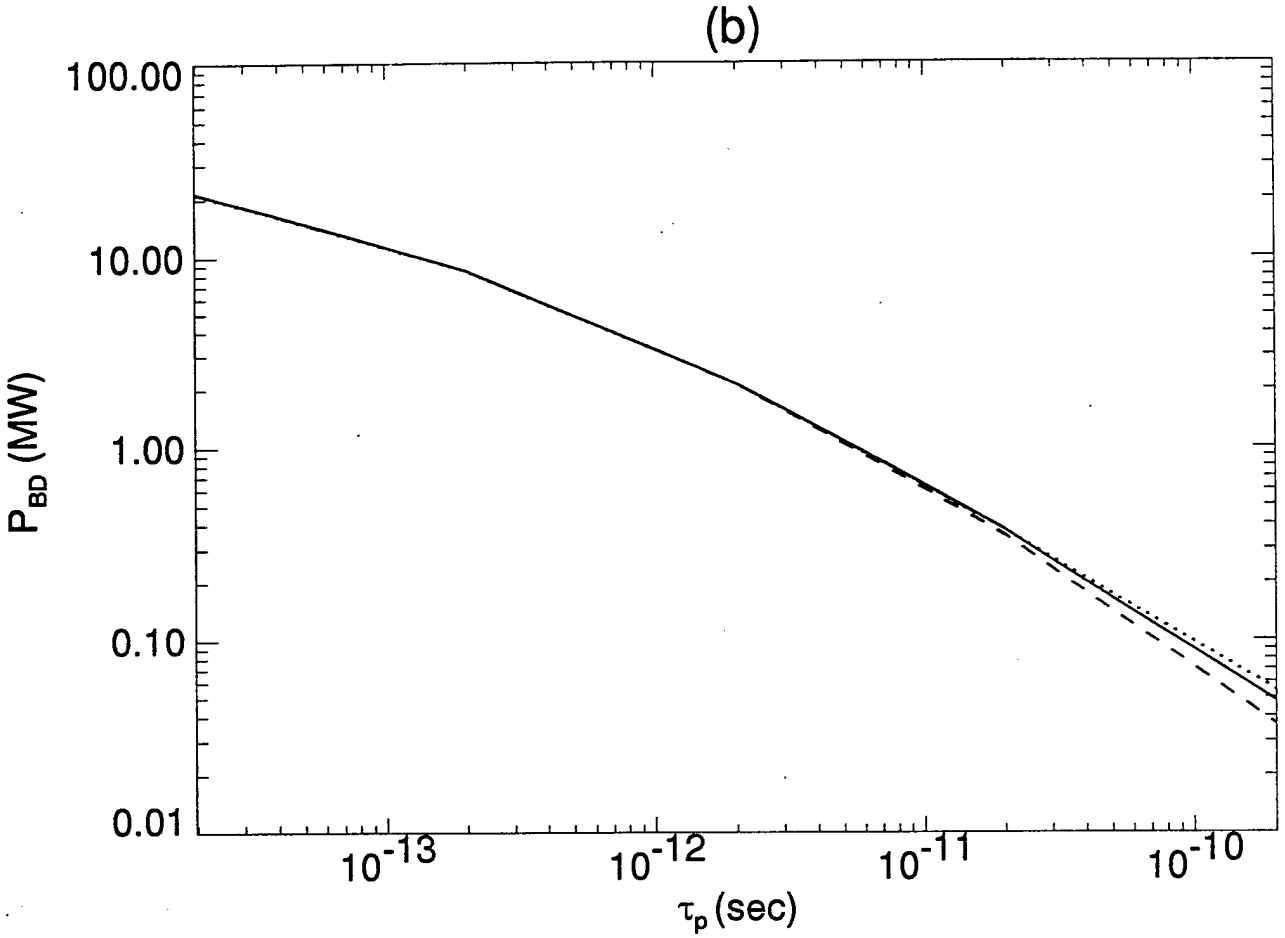

Figure 5

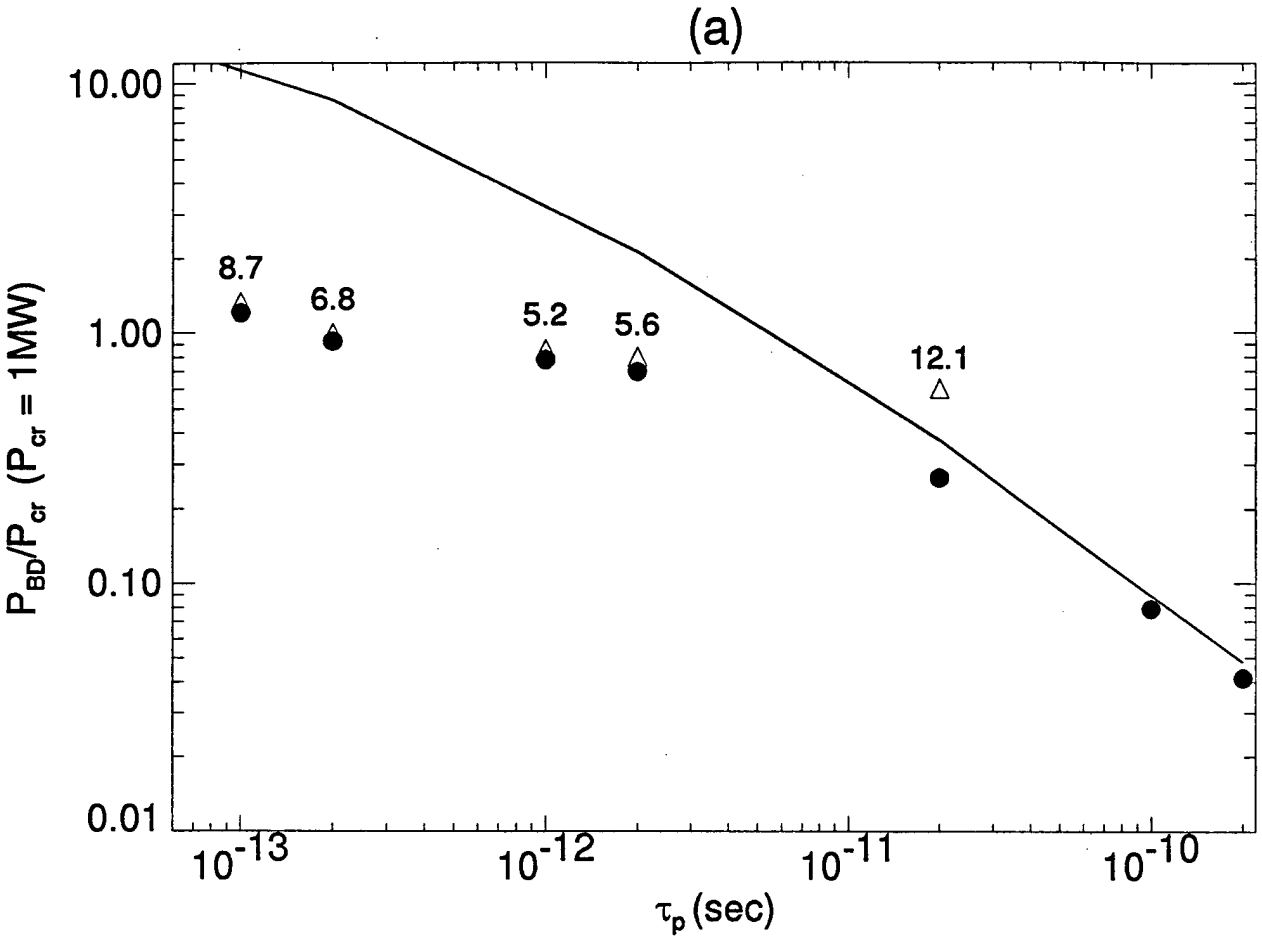
(a)
10.00
1.00
0.10
0.01
P_{BD}/P_{cr} (P_{cr} = 1MW)
8.7
6.8
5.2
5.6
12.1
10^{-13}
10^{-12}
10^{-11}
10^{-10}
τ_p (sec)

Figure 5

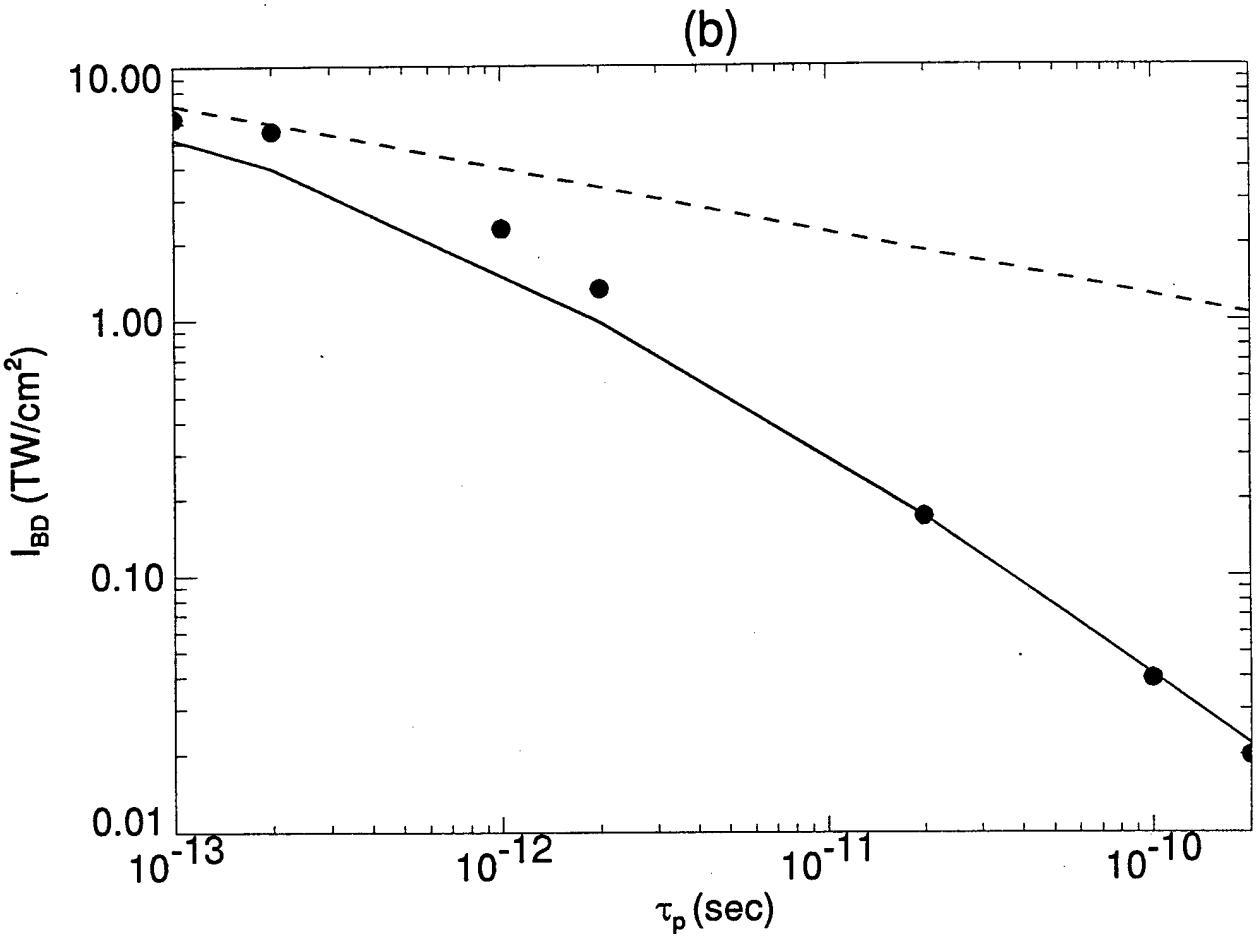

Figure 6

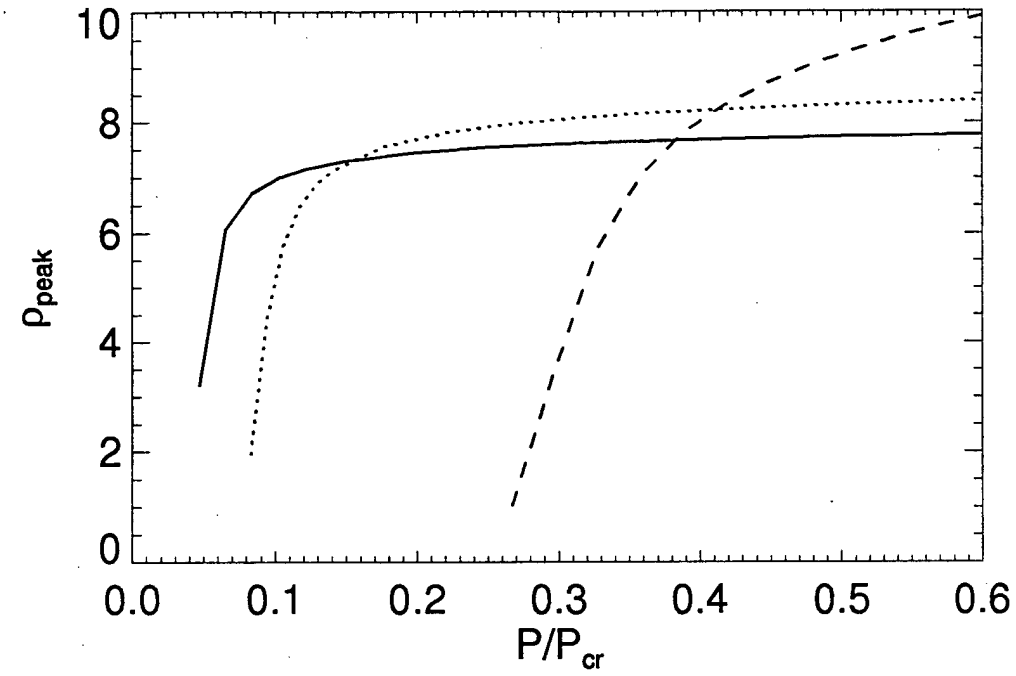
10
8
6
4
2
0
ρ_{peak}
0.0
0.1
0.2
0.3
0.4
0.5
0.6
P/P_{cr}

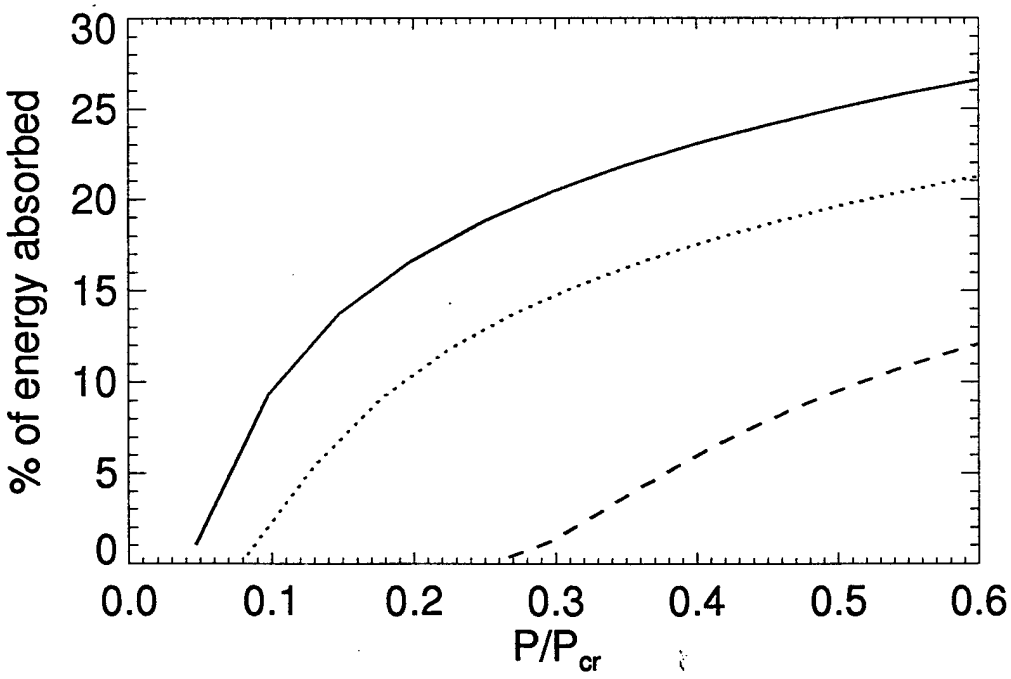
30
25
20
15
10
5
0
% of energy absorbed
0.0
0.1
0.2
0.3
0.4
0.5
0.6
P/P_{cr}

Figure 7

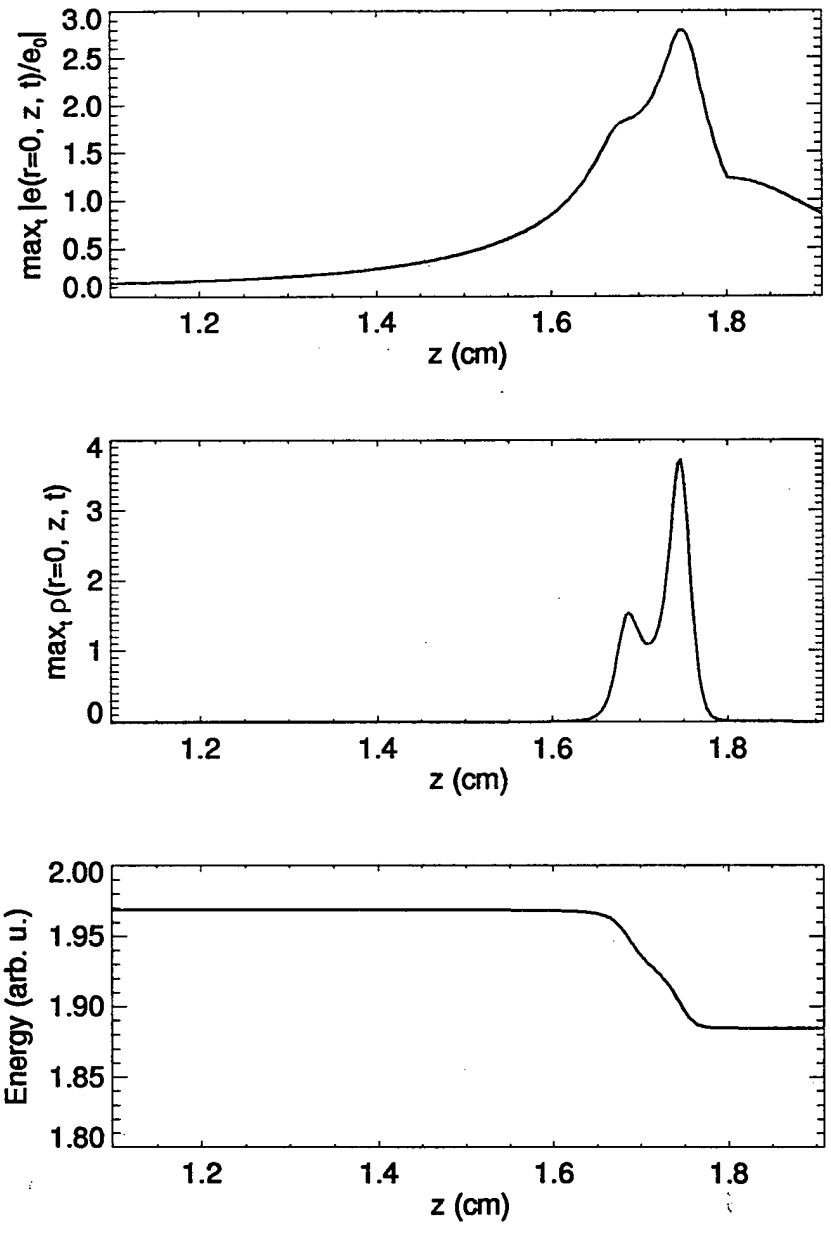
max$_t$ |e(r=0, z, t)/e$_0$|
3.0
2.5
2.0
1.5
1.0
0.5
0.0
1.2
1.4
1.6
1.8
z (cm)
max$_t$ ρ(r=0, z, t)
4
3
2
1
0
1.2
1.4
1.6
1.8
z (cm)
Energy (arb. u.)
2.00
1.95
1.90
1.85
1.80
1.2
1.4
1.6
1.8
z (cm)

Figure 8

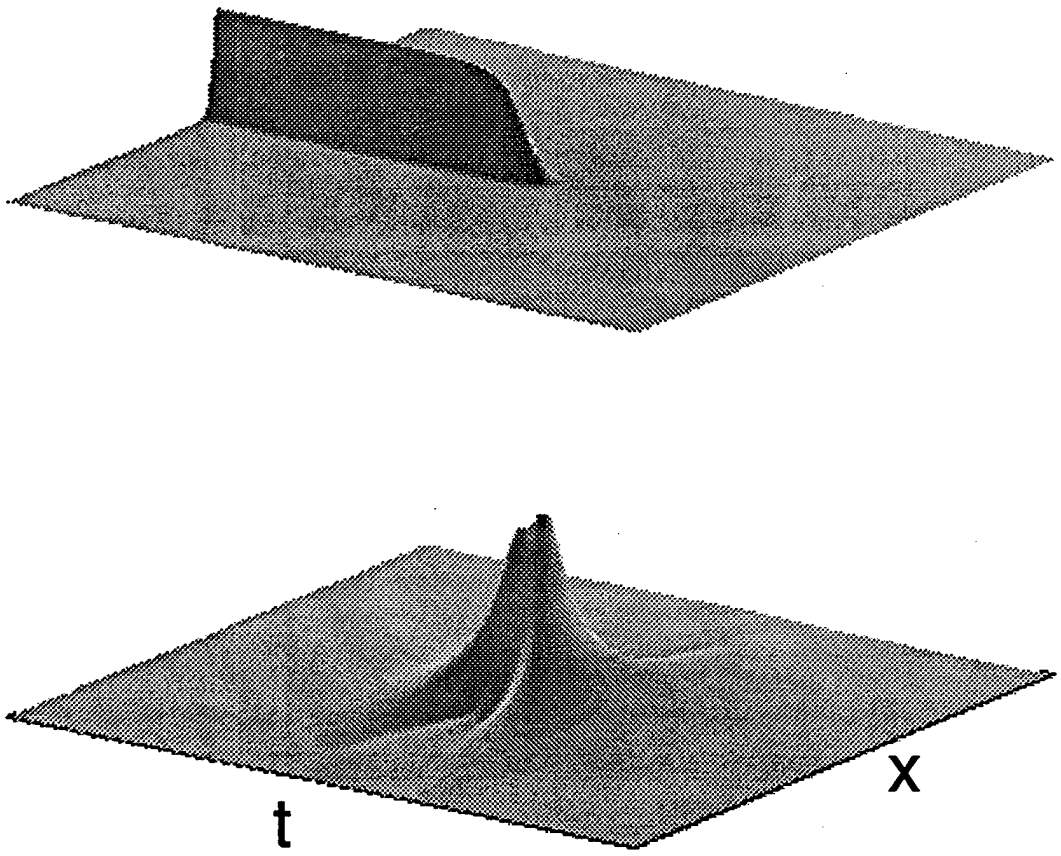

Figure 8

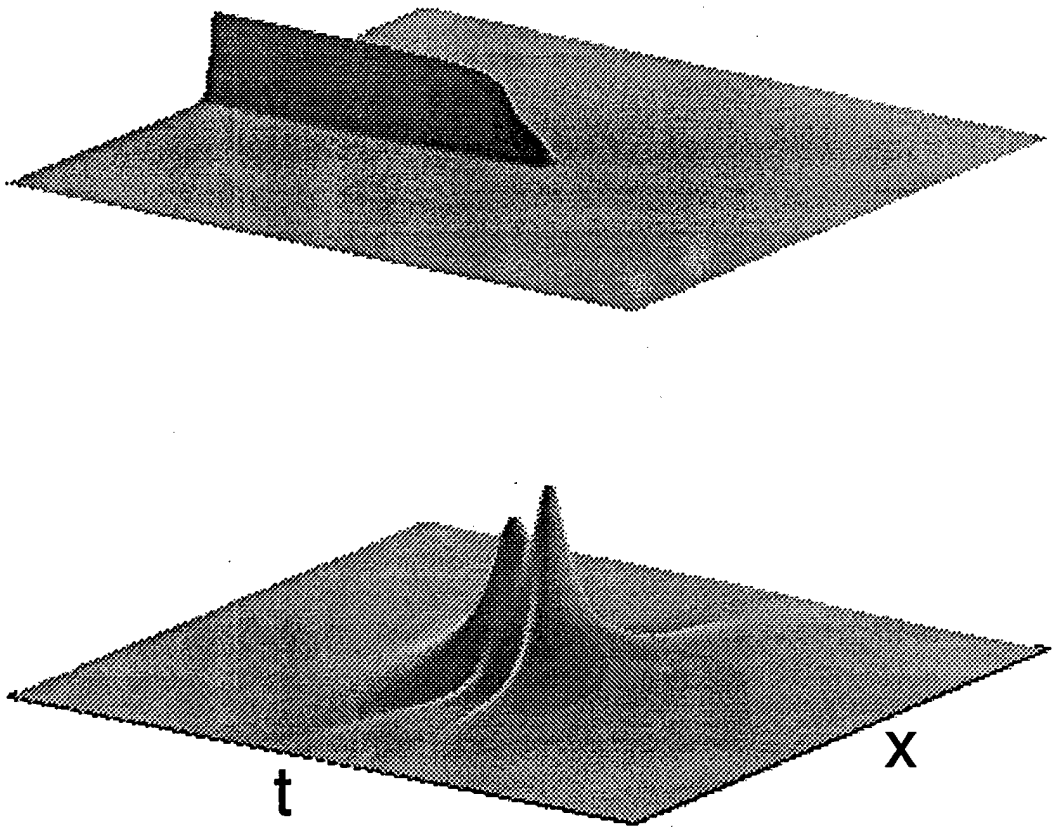

Figure 8

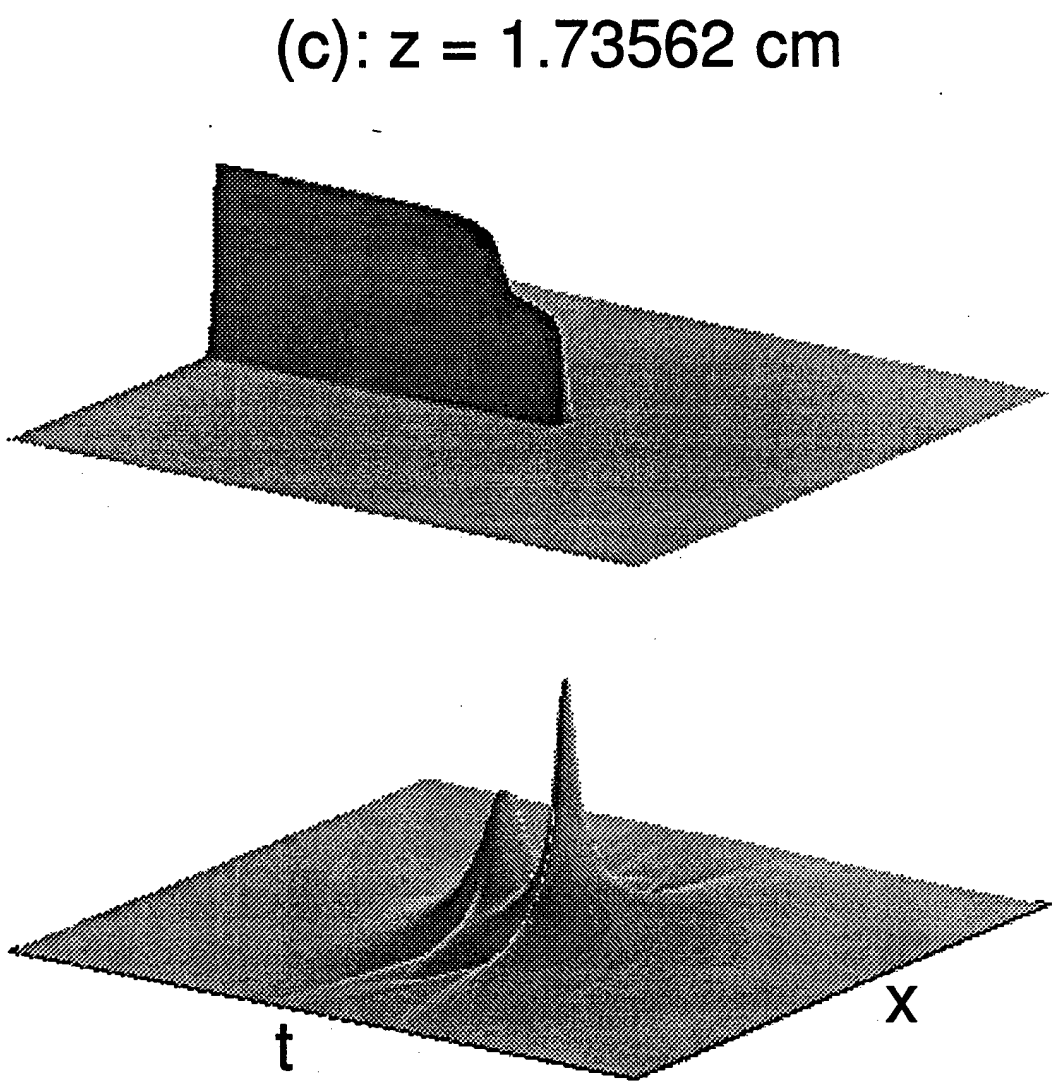

Figure 9

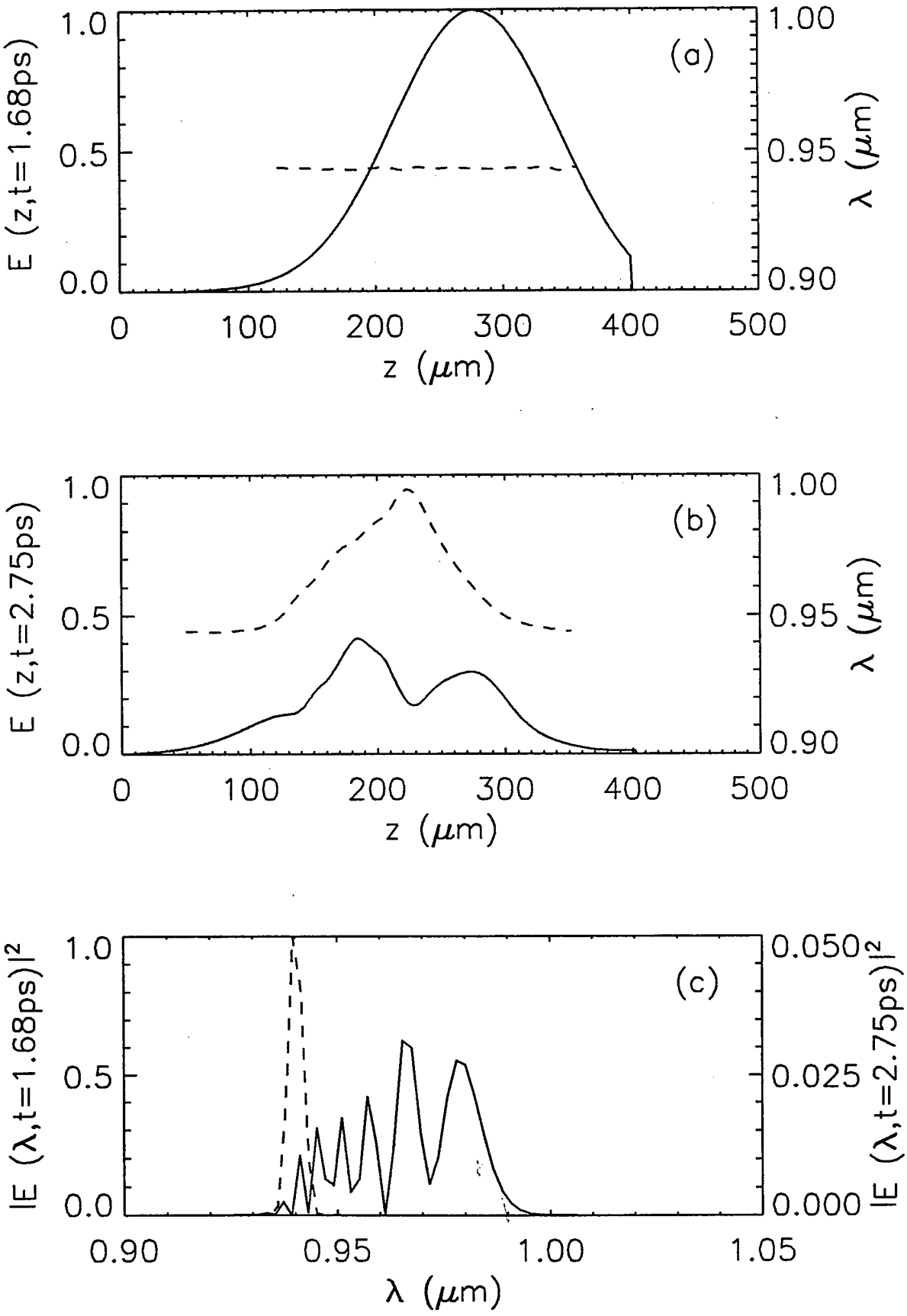
(a)
E (z,t=1.68ps)
λ (μm)
z (μm)
1.0
0.5
0.0
1.00
0.95
0.90
0
100
200
300
400
500
(b)
E (z,t=2.75ps)
λ (μm)
z (μm)
(c)
|E (λ,t=1.68ps)|²
|E (λ,t=2.75ps)|²
λ (μm)
0.050
0.025
0.000
0.90
0.95
1.00
1.05

Figure 10

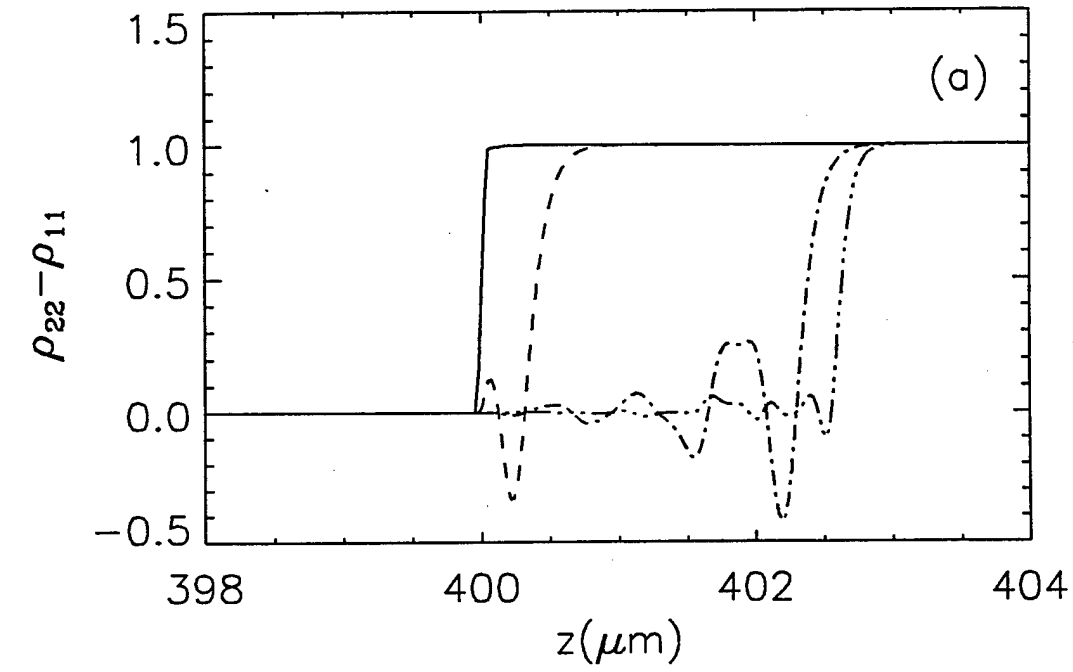
(a)
1.5
1.0
0.5
0.0
−0.5
$\rho_{22}-\rho_{11}$
398
400
402
404
z(μm)

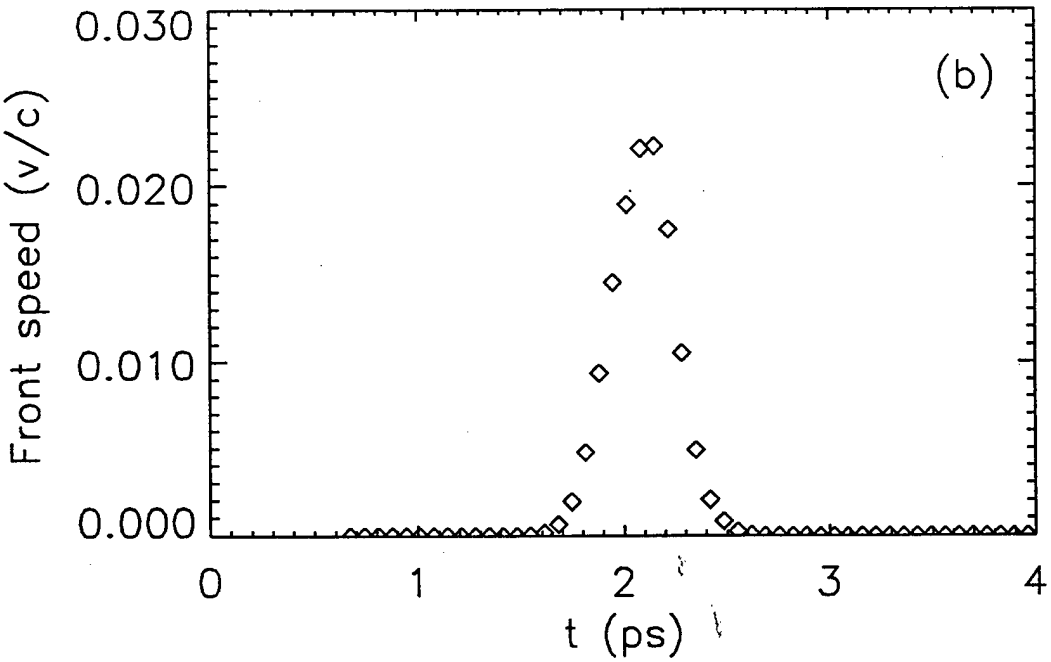
(b)
0.030
0.020
0.010
0.000
Front speed (v/c)
0
1
2
3
4
t (ps)

Theory and Simulation on the Threshold of Water Breakdown Induced by Focused Ultrashort Laser Pulses

Q. Feng, J. V. Moloney, A. C. Newell, E. M. Wright, K. Cook, P. K. Kennedy, D. X. Hammer, B. A. Rockwell, and C. R. Thompson

Abstract— **A comprehensive model is developed for focused pulse propagation in water. The model incorporates self-focusing, group velocity dispersion, and laser-induced breakdown in which an electron plasma is generated via cascade and multiphoton ionization processes. The laser-induced breakdown is studied first without considering self-focusing to give a breakdown threshold of the light intensity, which compares favorably with existing experimental results. The simple study also yields the threshold dependence on pulse duration and input spot size, thus providing a framework to view the results of numerical simulations of the full model. The simulations establish the breakdown threshold in input power and reveal qualitatively different behavior for pico- and femto-second pulses. For longer pulses, the cascade process provides the breakdown mechanism, while for shorter pulses the cooperation between the self-focusing and the multiphoton plasma generation dominates the breakdown threshold.**

I. Introduction

THE NONLINEAR optical properties of liquid water are of considerable interest [1], [2] due to their implications for pulse propagation in the human eye, the vitreous humor being predominantly water. Water displays a nonlinear Kerr effect [2], [3], and self-focusing (SF) can occur at megawatt peak input powers. In addition to SF, water also displays laser-induced breakdown (LIB) [4]–[6] in which an electron plasma is generated due to the high intensity of focused laser pulses. The electron density grows explosively and serves to absorb and scatter the remaining pulse energy, thus shielding the area beyond the focus from further radiation, i.e., the retina [7]–[10]. Indeed, SF leading to LIB has been suggested as the explanation for anomolies in the retinal damage data for visible femtosecond pulses [11]–[13]. Nonlinear pulse propagation in water is therefore of considerable interest in determining laser safety standards in the ultrashort pulse regime.

Manuscript received April 8, 1996; revised September 9, 1996. The work of Q. Feng, J. V. Moloney, E. W. Wright, and A. C. Newell was supported by the Air Force Office of Scientific Research, Air Force Materiel Command, USAF, under Grants F49620-94-1-0463 and F49620-94-1-0051. E. M. Wright was supported in part by the Joint Services Optical Program.

Q. Feng, J. V. Moloney, and A. C. Newell are with the Arizona Center for Mathematical Sciences, University of Arizona, Tucson, AZ 85721 USA.

E. M. Wright and K. Cook are with the Optical Sciences Center, University of Arizona, Tucson, AZ 85721 USA.

P. K. Kennedy, D. X. Hammer, and B. A. Rockwell are with the Optical Radiation Division, Armstrong Laboratory, Brooks AFB, San Antonio, TX 78235 USA.

C. R. Thompson is with Operational Technologies, Inc., Armstrong Laboratory, Brooks AFB, San Antonio, TX 78235 USA.

Publisher Item Identifier S 0018-9197(97)00957-3.

In this paper, we report numerical results on linear and nonlinear propagation in liquid water using 200-ps to 100-fs duration pulses. We consider a geometry in which a Gaussian input field is focused through a lens into the water sample, thus simulating to first order the focusing properties of the eye. The studies incorporate LIB, SF, multiphoton absorption (MPA), and group velocity dispersion (GVD). The model is an extended nonlinear Schrödinger equation (NLSE) coupled with an equation describing the plasma generation. The NLSE is widely used to describe light propagation and has been studied extensively [14]. An interesting mechanism modeled by the NLSE is self-focusing and beam collapse. When a focused or unfocused propagating laser beam undergoes self-focusing, the on-axis intensity gets enhanced considerably if the power of the beam is near but below a critical value. When the power is above the critical value, the collapse, namely an infinitely high intensity, occurs at finite propagation distance. The collapse is clearly unphysical and one would expect other nonlinear effects, such as material breakdown, to come into play due to the high intensity produced. Here, we extend the NLSE to include plasma generation, pulse–plasma interaction, and MPA. The plasma generation is described by two processes: cascade (or avalanche) ionization and multiphoton ionization. Included also is the GVD, which has been shown to lead to pulse-spliting and to arrest the collapse of subpicosecond pulses [15]–[21]. Two focusing mechanisms exist in our studies: linear focusing, due to the lens, and nonlinear self-focusing. A framework for these studies is provided by first studying LIB without SF, and this model compares favorably with existing experimental results. We then establish a threshold for LIB by numerical simulations. Our results show that SF is a major player in understanding LIB in water for pulses of the durations considered in this paper and of spot-sizes that can be easily determined from a criterion given in this paper.

The remainder of this paper is organized as follows. In Section II, we describe the model equations, the focusing geometries and material parameters pertinent to experiments, and write the equations into dimensionless form with appropriate scalings. Although we will present our results in subsequent sections in physical units to facilitate comparison with experiments, a quick inspection of the dimensionless equations leads to an interesting and important result, i.e., the relation of the breakdown threshold intensity to the pulse duration for the case where multiphoton ionization is the

1994

Reprinted from

E. M. Wright

PHYSICA D

Physica D 74 (1994) 59–73

The effects of normal dispersion on collapse events

G.G. Luther, A.C. Newell, J.V. Moloney

Arizona Center for Mathematical Sciences, Department of Mathematics, University of Arizona, Tucson, Arizona 85721, USA

Received 10 August 1993; revised 21 December 1993; accepted 21 December 1993
Communicated by V.E. Zakharov

N·H

Self-focusing threshold in normally dispersive media

G. G. Luther,* J. V. Moloney, and A. C. Newell

Arizona Center for Mathematical Sciences, Department of Mathematics, University of Arizona, Tucson, Arizona 85721

E. M. Wright

Optical Sciences Center and Department of Physics, University of Arizona, Tucson, Arizona 85721

Received November 23, 1993

The threshold at which self-focusing initially dominates the dynamics of short-pulse propagation in normally dispersive bulk media, causing an explosive increase in peak intensity, is estimated analytically and verified numerically. Intensity-dependent propagation effects such as spectral broadening also occur explosively at this threshold.

It was recently proposed by Strickland and Corkum[1] that normal group-velocity dispersion (GVD) increases the peak input power required for two-dimensional (2D) self-focusing of short light pulses. Their proposal is intriguing since it provides a limiting mechanism that does not require higher-order nonlinear effects, such as saturation of the nonlinear refractive index,[2] optical breakdown,[3] and violation of the paraxial approximation.[4]

Because cross sections of a light pulse differ in power, those having powers that exceed the critical power self-focus at different rates. In this way, self-focusing tends to reduce the temporal scale length of a pulse,[5,6] with concomitant increase in its bandwidth, permitting GVD to play an increasingly important role even when it is initially a small effect.[7]

Normal GVD tends to ease self-focusing by spreading the pulse along the propagation direction. Recent numerical studies of the nonlinear Schrödinger equation by Chernev and Petrov[8] and Rothenberg[9] demonstrate that normal GVD increases the threshold for catastrophic 2D self-focusing through a temporal pulse-splitting process. Analytic research has shown that the critical self-similar collapse singularity associated with the 2D nonlinear Schrödinger equation is removed by normal dispersion.[10]

The simplest and most ubiquitous model of the spatiotemporal propagation of a light pulse is obtained as a uniform asymptotic expansion of Maxwell's equations. If we take the nonlinear response of the medium to be instantaneous and centrosymmetric, the nonlinear Schrödinger equation for the envelope of a light pulse is obtained as[1,9]

$$2ik\left(\frac{\partial A}{\partial z}+\frac{\partial k}{\partial \omega}\frac{\partial A}{\partial t}\right)+\nabla_{\perp}^{2}A-k\frac{\partial^{2}k}{\partial \omega^{2}}\frac{\partial^{2}A}{\partial t^{2}}+2k^{2}\frac{n_{2}}{n_{0}}|A|^{2}A=0. \quad (1)$$

We have conducted extensive numerical simulations of Eq. (1) with $n_2 > 0$, $\partial^2 k/\partial\omega^2 > 0$, and initial data of the form $A(x, y, z = 0, t) = \exp[-(x^2 + y^2)/2w_0^2 - t^2/2t_p^2]$ to explore the dynamics of pulse propagation. Results with the split-step method[11] were checked against previous numerical simulations.[8,9,12] The first three invariants of motion and the magnitude of higher-order corrections were monitored carefully. In the simulations discussed here, nonparaxial effects remained small. These numerical experiments show that, as the peak input power is increased, a threshold P_{TH} is reached[8] where self-focusing dominates the initial dynamical evolution of the pulse. Near P_{TH} the pulse-splitting process coincides with the arrest of the collapse at the peak of a pulse. In this Letter it is shown that P_{TH} corresponds to the input power at which the length scale for self-focusing equals the length scale for nonlinear dispersion. In addition, an expression for P_{TH} is derived analytically and verified numerically.

A consequence of the sharp increase in peak intensity at threshold is the observation of intensity-dependent processes. An important example is the explosive spectral broadening that occurs near P_{TH}. Through four-wave coupling of the wave trains that make up the pulse, a nonlinear chirp is formed along the pulse. As a result, upshifted and downshifted wave packets form under the pulse. The two wave packets eventually separate in the presence of normal dispersion, splitting the pulse. The spectrum of the resulting double-peaked pulse is broadband and modulated.[1,9] This process occurs over a short propagation length near the self-focusing threshold, resulting in an explosive increase of the bandwidth. The bandwidth increases more than would be expected by self-phase modulation in time. The gain in the four-wave interaction that is responsible for the broadening is favored for off-axis, frequency-shifted modes.[13] Neither pulse splitting nor this enhancement in the spectral broadening is captured by either stationary self-focusing or one-dimensional propagation alone.

The solutions of Eq. (1) are functions of only two parameters when Gaussian initial data are used. We have chosen to write the first parameter as $\gamma = L_{DF}/L_{DS}$, which measures the strength of the dispersion relative to diffraction, where $L_{DS} = t_p^2/k''$

0146-9592/94/120862-03$6.00/0

Short-pulse conical emission and spectral broadening in normally dispersive media

G. G. Luther,* A. C. Newell, and J. V. Moloney

Arizona Center for Mathematical Sciences, Department of Mathematics, University of Arizona, Tucson, Arizona 85721

E. M. Wright

Optical Sciences Center and Department of Physics, University of Arizona, Tucson, Arizona 85721

Received January 4, 1994

The nonlinear Schrödinger equation predicts conical emission that is due to spatiotemporal propagation of short pulses in normally dispersive, cubically nonlinear media. This effect is a direct consequence of a four-wave interaction.

Conical emission has long been associated with spectral superbroadening[1] (SSB) and has been attributed to four-photon coupling.[2] Recent laboratory[3] experiments demonstrate that SSB correlates with the threshold for self-focusing (SF). Both these laboratory experiments and several numerical experiments[4–8] suggest that SF is inhibited by normal group-velocity dispersion (NGVD), and the threshold required for the observation of strong SF effects is increased,[5,6] having a simple analytical form.[7] Near this threshold SSB, conical emission, and pulse splitting[5] occur explosively. Here we show that conical emission is a direct consequence of the spatiotemporal dynamics of short laser pulses described by the nonlinear Schrödinger equation

$$2ik\left(\frac{\partial A}{\partial z}+\frac{\partial k}{\partial \omega}\frac{\partial A}{\partial t}\right)+\nabla_{\perp}{}^{2}A-k\frac{\partial^{2}k}{\partial \omega^{2}}\frac{\partial^{2}A}{\partial t^{2}}+2k^{2}\frac{n_{2}}{n_{0}}|A|^{2}A=0, \qquad (1)$$

where $k''=\partial^{2}k/\partial\omega^{2}|_{\omega 0}>0$ for NGVD. The conical emission predicted by Eq. (1) is due to a fundamental four-wave interaction[9] that promotes the transport of energy to a band of modes with finite frequency and wave-number shifts. These modes are closely related to those of the modulational instability of the condensate or the uniform plane-wave solution.[10] Pulse splitting, spectral broadening, and conical emission are intimately related, and each is a consequence of this wave interaction.

For short pulses, corrections to Eq. (1) appear at the next order in the uniform asymptotic expansion and account for self-steepening, stimulated Raman scattering, exponential finite-time nonlinear response,[11] higher-order dispersion, nonparaxial effects,[12] and vector contributions. Terms in the next order beyond those appearing in Eq. (1) introduce asymmetries in time and in frequency space. Below the threshold reported in Ref. 7 these effects introduce small corrections that become important only at propagation distances larger than those required for pulse splitting and conical emission. We neglect higher-order effects and focus on the characteristics properties of the conical emission captured by Eq. (1).

First we demonstrate the growth of frequency-shifted, off-axis modes numerically at parameter values below the threshold reported in Ref. 7 and above the stationary SF threshold, P_c. For the parameters of interest here, the space and time dynamics are strongly coupled, and standard analytic technique fail. The split-step method[13] is used to integrate Eq. (1) with initial data of the form $A(x,y,z=0,t)=\exp[-(x^{2}+y^{2})/w_{0}{}^{2}-(t/t_{p})^{2}]$, where w_0 is the beam width and t_p is the pulse length. The parameters were chosen so that $L_{\mathrm{DF}}k''/t_{p}{}^{2}=0.1$ and $P/P_c=1.5$, where $L_{\mathrm{DF}}=w_{0}{}^{2}k/2$ and P_c is the critical power for two-dimensional SF. In Fig. 1 the contours of the intensity, $|A(x,y=0,t)|^{2}$, and the far-field spectrum, $\log[|A(k_x,k_y=0,\omega)|]$, are displayed for $z=0.0$, 1.1, and 1.5 times the diffraction length, L_{DF}. Figure 1(a) shows the initial pulse as it enters the medium. Its spectrum is localized, appearing oval in (ω,k_x). In Fig. 1(b) the pulse has propagated into the medium, reaching a stage just before the splitting event. A four-wave interaction has transported energy from the band of wave trains, (k,ω), to sidebands at $(k_x\pm\kappa_x,k_y\pm\kappa_y,\omega\pm\Omega)$. The interaction broadens the spectrum in both frequency and wave number, but it is most efficient along curves for which $\Omega^{2}\propto k_{\perp}{}^{2}$, where $k_{\perp}=(\kappa_x,\kappa_y)$. The four-wave interaction that produces this new spectral feature dominates the spectral broadening process. In Fig. 1(c) the pulse has split. A faint indication of modulations in the frequency spectrum can be seen, which at higher values of the initial power are readily apparent.[5] Analogous spatiotemporal four-wave interactions destabilize both the condensate[10] and the cw beam[14] solutions of Eq. (1).

A consequence of the growth of this new spectral feature is the appearance of frequency-shifted off-axis radiation in the far-field image of the pulse, which

0146-9592/94/110789-03$6.00/0

Carrier Wave Shocking of Femtosecond Optical Pulses

R. G. Flesch, A. Pushkarev, and J. V. Moloney
Arizona Center for Mathematical Sciences, Department of Mathematics, University of Arizona, Tucson, Arizona 85721
(Received 20 June 1995)

Numerical integration of Maxwell's equations for propagation of a femtosecond pulse in a medium with linear Lorentz response and a Kerr nonlinearity shows shock formation on the underlying carrier wave prior to the envelope shock. The carrier shock is characterized by the appearance of a strong third harmonic pulse, whereas the envelope shock appears later as spectral broadening and modulation of the fundamental and higher harmonic spectral features.

PACS numbers: 42.65.Ky

Advances in laser technology in the past decade have made possible the production of pulses which contain a few optical cycles [1]. Although such ultrashort pulses contain small amounts of optical energy, enormous intensities exceeding 1 TW/cm^2 can arise and the accompanying intensity-dependent corrections to the index of refraction are such that one can expect novel nonlinear phenomena such as shock formation over very short propagation lengths. It has been suggested in [2] that an envelope shock was observed experimentally [3] and that this can be understood using standard envelope approximations [2,4] to Maxwell's equations. Laser-induced breakdown (LIB) cannot be ruled out at such very high peak intensities, but there is evidence to show that for such short and hence low energy pulses the cascade-avalanche path is unlikely and multiphoton processes are more likely to lead to breakdown [5]. Indeed, very recent experiments in water using 100 fs pulses indicate that local peak field intensities can exceed 10^{13} W/cm^2 in the focal region with incident pulse absorption being less than 5% [6]. Moreover, breakdown becomes a sensitive function of optical wavelength. Shock formation on the carrier wave is expected therefore to compete with other physics during the critical collapse of femtosecond duration optical pulses in optically transparent media where the local intensity at the critical collapse distance can become very large.

The above breakdown scenario is extremely complicated, so we confine our attention here to plane wave propagation for simplicity and show that an optical carrier shock can arise in a medium with an instantaneous Kerr nonlinearity. Dispersion plays an important role in shock regularization (smoothing) and influences the signature of the carrier shock. As dispersion is typically strong for such short optical pulses [the dispersion length scales as k''/τ_p^2, where k'' is the leading order contribution to the group velocity dispersion (GVD) and τ_p is the characteristic pulse length], phase mismatch leads to the separation in time of a strong third harmonic optical pulse moving with a different group velocity from the fundamental. For very weak dispersion, a component of the third harmonic pulse moves with the fundamental and, in the dispersionless case, all higher harmonics of the fundamental are phase matched and see explosive growth. As the phenomena we are concerned with occurs on the scale of the carrier wavelength, no envelope approximations are valid and one must resort to a numerical integration of Maxwell's equations. Numerical schemes for the integration of Maxwell's equations have been refined in the past few years [7] to allow for an efficient integration of media with memory in both the linear and nonlinear polarizations.

We restrict our attention to nonmagnetic dielectric media with no free charges, in which case we have for Maxwell's equations

$$\frac{\partial B_y}{\partial t} = \frac{\partial E_x}{\partial z}, \qquad \frac{\partial D_x}{\partial t} = \frac{1}{\mu_0}\frac{\partial B_y}{\partial z}, \tag{1}$$

where all quantities above and in the following are in MKS units. The medium is modeled by a single Lorentz oscillator plus an instantaneous Kerr nonlinearity

$$D_x(z,t) = \epsilon_0\left\{\varepsilon_\infty E_x(z,t) - \int_{-\infty}^{t} dt'\,\chi(t-t')E_x(z,t') + \chi^{(3)}E_x^3(z,t)\right\}, \tag{2}$$

with the linear susceptibility given by $\chi(t) = \omega_p^2 e^{-\delta t/2} \times \sin(\sqrt{\omega_0^2 - \delta^2/4}\,t)/\sqrt{\omega_0^2 - \delta^2/4}$, $[\hat{\chi}(\omega) = \omega_p^2/(\omega_0^2 - i\delta\omega - \omega^2)]$, $\omega_p^2 = (\varepsilon_s - \varepsilon_\infty)\omega_0^2$, ε_s and ε_∞ are the static and infinite relative permittivities, respectively, and ω_0 the resonance frequency of the Lorentz oscillators. Maxwell's equations are solved by either a second order in time, second order in space [(2,2)] finite difference time domain method [8] or a second order in time, fourth order in space [(2,4)] scheme [9]. The numerical dispersion inherent in these methods has recently received a good deal of attention [10], and we have chosen our spatial discretizations accordingly.

The convolution integral $P_L = \epsilon_0 \int dt'\,\chi(t-t')E_x(t')$ in Eq. (2) is most efficiently solved by replacing it with the equivalent second order ordinary differential equation [7,11]

$$\frac{1}{\omega_0^2}\frac{d^2P_L}{dt^2} + \frac{\delta}{\omega_0^2}\frac{dP_L}{dt} + P_L = \frac{\omega_p^2}{\omega_0^2}\epsilon_0 E_x, \tag{3}$$

which is solved by second order central differencing.

0031-9007/96/76(14)/2488(4)$10.00

Laser-induced breakdown versus self-focusing for focused picosecond pulses in water

Q. Feng, J. V. Moloney, and A. C. Newell

Arizona Center for Mathematical Sciences, University of Arizona, Tucson, Arizona 85721

E. M. Wright

Optical Sciences Center, University of Arizona, Tucson, Arizona 85721

Received May 11, 1995

We present numerical studies of nonlinear propagation for picosecond pulses focused in water. Depending on the pulse duration and focusing conditions, for some input powers self-focusing may precede laser-induced breakdown and vice versa. We derive a criterion that predicts the relative roles of laser-induced breakdown and self-focusing. © 1995 Optical Society of America

The nonlinear-optical properties of liquid water are of considerable interest[1,2] owing to their implications for propagation in the eye, the vitreous humor being predominantly water. Water displays self-focusing (SF) at megawatt input powers[2,3] and has been suggested as the source of retinal damage at anomolously low energies for femtosecond pulses.[4] Water also displays laser-induced breakdown (LIB),[5–7] in which an electron plasma grows exponentially by avalanche ionization.[6] Once generated, this electron plasma serves to absorb and scatter the remaining pulse energy, thus effectively shielding the area beyond the plasma, i.e., the retina.[8–11] The interplay between SF and LIB is therefore of importance in assessing laser eye damage.

In this Letter we report numerical simulations of SF and LIB in water using picosecond pulses. Our numerical simulations revealed cases of peak input powers for which SF preceded LIB and vice versa, depending on the pulse duration and focusing conditions (see also Refs. 2, 12, and 13). Here we develop a critical power P_{LIB} for LIB that can be compared with the critical power P_{cr} for SF: For $P_{\mathrm{LIB}} > P_{\mathrm{cr}}$, SF precedes LIB; for $P_{\mathrm{LIB}} < P_{\mathrm{cr}}$, LIB precedes SF. Numerical simulations are presented to show that this criterion predicts the correct dependence on focal length and pulse duration.

Our theoretical model for LIB is that previously described by Feit and Fleck[14] appropriately extended to include nonlinear SF.[15] The equation for the electric-field envelope $\mathcal{E}(r, z, t)$ in a reference frame moving at the group velocity is then

$$\frac{\partial \mathcal{E}}{\partial z} = \frac{i}{2k}\nabla_T^2 \mathcal{E} - \frac{\sigma}{2}(1 + i\omega\tau)n\mathcal{E} + ik_0 n_2 |\mathcal{E}|^2 \mathcal{E}, \tag{1}$$

along with the following Drude model describing avalanche ionization of the electron density n (Ref. 6):

$$\frac{\partial n}{\partial t} = (\ln 2)\frac{\sigma}{E_g} n|\mathcal{E}|^2 - an^2. \tag{2}$$

Here $|\mathcal{E}|^2$ is the intensity, $k = n_b k_0 = n_b \omega/c$, n_2 is the nonlinear coefficient, σ is the cross section for electron-neutral inverse bremsstrahlung, τ is the electron collision relaxation time, E_g is the ionization energy, and a is the rate of radiative recombination. Here we consider the following parameter values appropriate to the visible wavelength $\lambda_0 = 580$ nm: $\tau = 10^{-15}$ s,[16] $n_b = 1.33$, $n_2 = 2 \times 10^{-16}$ cm^2/W,[3] $E_g = 6.5$ eV,[16] $a \approx 10^{-9}$ cm^3 s^{-1},[17] and $\sigma = 1.4 \times 10^{-17}$ cm^2.[14] The critical power for SF is $P_{\mathrm{cr}} = 0.15\lambda^2/n_b n_2$, which yields $P_{\mathrm{cr}} = 2$ MW for the above parameters.[2]

We are interested in the solutions of Eqs. (1) and (2) for an initial Gaussian beam focused onto the water sample through a lens of focal length f,

$$\mathcal{E}(r, 0, t) = \sqrt{\frac{2P_{\mathrm{in}}}{\pi w_0^2}} \exp\left(-\frac{r^2}{w_0^2} - \frac{t^2}{t_p^2} - \frac{ikr^2}{2f}\right), \tag{3}$$

where P_{in} is the peak power, w_0 is the spot size, and t_p is the pulse length. In the absence of LIB the behavior of the field is dictated by the power ratio $P_{\mathrm{in}}/P_{\mathrm{cr}}$ since each time slice of the pulse acts independently.[15] For $P_{\mathrm{in}}/P_{\mathrm{cr}} > 1$ the central time slice of the pulse undergoes collapse to a singularity at a nonlinear focal distance

$$\frac{1}{f_{\mathrm{NL}}} = \frac{1}{f} + \frac{1}{z_{\mathrm{NL}}(P_{\mathrm{in}})}, \tag{4}$$

where $z_{\mathrm{NL}}(P_{\mathrm{in}})$ is the nonlinear collapse distance without the lens.[15] For $P_{\mathrm{in}}/P_{\mathrm{cr}} = 1$ we have $z_{\mathrm{NL}} \to \infty$, so that the field collapses at the linear focus.

Our numerical simulations based on Eqs. (1) and (2) show that LIB prevents catastrophic SF to a singularity by absorption and defocusing of the incident field that result from the electron plasma.[14] However, SF can proceed a considerable distance into the collapse before it is arrested by LIB. To obtain a criterion for the relative roles of SF and LIB we neglect the effects of SF. Then the input Gaussian field will come to a focus at a longitudinal position $d = f/(1 + f^2/z_0^2)$,[16] where $z_0 = \pi w_0^2 n_0/\lambda_0$ is the Rayleigh range of the input beam. The size of the laser beam w_f at the focus is $(w_f/w_0)^2 = (f^2/z_0^2)/(1 + f^2/z_0^2) = z_f/z_0$, with z_f the Rayleigh range of the focused beam. To obtain a criterion for LIB we use the following model: The laser

0146-9592/95/191958-02$6.00/0

Nonlinear focusing of femtosecond pulses as a result of self-reflection from a saturable absorber

W. Forysiak and J. V. Moloney

Arizona Center for Mathematical Sciences, Department of Mathematics, University of Arizona, Tucson, Arizona 85721

E. M. Wright

Optical Sciences Center, University of Arizona, Tucson, Arizona 85721

Received September 9, 1996

We calculate the spatiotemporal evolution of intense, femtosecond pulses that are incident upon a saturable absorbing interface in the regime of self-reflection, using the finite-difference time-domain computational method. The pulses induce a curved, moving absorption front in the nonlinear medium that acts as a transient focusing mirror for the reflected pulse energy. © 1997 Optical Society of America

The propagation of an intense optical field that is incident from air upon a saturable absorber can give rise to a self-reflected wave if the absorption is sufficiently large.[1] The reflected wave arises at a wavelength-scale spatial transition between the saturated and the unsaturated regions of the absorber,[2] akin to the skin effect at a linear boundary, and is self-reflected in the sense that the transition region is induced by the incident field itself. The self-reflected wave first predicted for a cw incident plane-wave field[1] was subsequently extended to consideration of a cw incident beam with a Gaussian transverse profile.[3] In the latter case the emergence of a halo was predicted in the far field at high intensities. Recently, the finite-difference time-domain (FDTD) method[4,5] was used to study the dynamics of self-reflection under pulsed excitation and to predict an intensity-dependent Doppler shift in the reflected pulse.[6]

In this Letter we include transverse variations to study the spatiotemporal dynamics of self-reflection. The FDTD method discretizes the differential form of Maxwell's equations directly and allows one to determine the evolution of an optical field in a nonlinear medium, subject to the given constitutive relations between the electric field and polarization (see, e.g., Refs. 7 and 8) and without recourse to the slowly varying envelope approximation. We examine pulse shaping in the near field, close to the absorber boundary, and predict a new nonlinear-focusing effect, which we attribute to the formation of a transient focusing mirror in the absorber. As the incident pulse impinges upon and strongly saturates the absorber, it excites a moving reflection front[6] that is shaped according to the transverse profile of the incident pulse. If the incident pulse's transverse profile is bell shaped, so too is the resulting mirror, and the reflected pulse is focused according to the waist and intensity of the incident pulse. In addition to being reshaped, the reflected pulse is spectrally broadened and red shifted owing to the Doppler effect at the moving mirror.[6]

We consider the time-dependent propagation of a two-dimensional TE-polarized pulse, in which the electric field is polarized along the y axis and is also assumed to be uniform along that axis, $E(r,t) = yE_y(x,z,t)$. Then the Maxwell equations for the electric and magnetic field quantities E_y, B_x, and B_z are

$$\frac{\partial B_x}{\partial t} = \frac{\partial E_y}{\partial z}, \quad \frac{\partial B_z}{\partial t} = \frac{\partial E_y}{\partial x}, \quad \frac{\partial D_x}{\partial t} = \frac{1}{\mu_0}\left(\frac{\partial B_x}{\partial z} - \frac{\partial B_z}{\partial x}\right), \tag{1}$$

where the z axis is the propagation direction and the x axis is the transverse direction. The nonlinear-optical response of the saturable absorber is included by use of a two-level model through the constitutive relation $D_y = \epsilon_0 E_y + P_y$, where the macroscopic polarization $P_y = Np(\rho_{21} + \text{c.c.})$ is determined by the Bloch equations[9]

$$\frac{\partial \rho_{21}}{\partial t} + (\gamma_2 + i\omega_{21})\rho_{21} = i\frac{pE_y}{\hbar}n, \qquad \frac{\partial n}{\partial t} + \gamma_1(n-1) = 2i\frac{pE_y}{\hbar}(\rho_{21} - \rho_{21}^*). \tag{2}$$

Here N is the density, ρ_{21} is the off-diagonal density matrix element, $n = (\rho_{11} - \rho_{22})$ is the population difference, ω_{21} is the transition frequency, p is the dipole moment, and $\gamma_1 = 1/t_1$ and $\gamma_2 = 1/t_2$ are the population and polarization damping constants, respectively.

The conditions for self-reflection of a continuous plane-wave incident field require that the normalized parameters $\psi = p^2N/\epsilon_0\hbar\gamma_2$ and $F = pE_0/\hbar(\gamma_1\gamma_2)^{1/2}$ be greater than unity, with E_0 the peak input field. Physically, this requires that the linear absorption be large, on a wavelength scale, and that the incident field be strong enough to saturate the absorption.[2] In the case of ultrashort pulses we also require that the incident pulse duration t_p be greater than the polarization decay time but less than the population decay time, $t_1 > t_p > t_2$.[6] To meet these conditions for the sub-100-fs pulses to which we were restricted by computational resources, we adopted the following medium parameters for illustrative purposes: $t_1 = 0.5$ ns, $t_2 = 10$ fs, $\omega = \omega_{21} = 2 \times 10^{15}$ rad s^{-1} ($\lambda = 942$ nm), $p = 4 \times 10^{-29}$ C, and $N_0 = 2 \times 10^{20}$ cm^{-3}. For these values a normalized field strength of $F = 1$ corresponds to an electric field strength of $E_0 =$

0146-9592/97/040239-03$10.00/0

Doppler Shift of Self-Reflected Optical Pulses at an Interface: Dynamic Nonlinear Optical Skin Effect

W. Forysiak,* R. G. Flesch, and J. V. Moloney
Arizona Center for Mathematical Sciences, Department of Mathematics, University of Arizona, Tucson, Arizona 85721

E. M. Wright
Optical Sciences Center, University of Arizona, Tucson, Arizona 85721
(Received 10 October 1995)

We introduce the dynamic nonlinear optical skin effect in which a pulse incident on a saturable absorbing interface is self-reflected from a moving absorption front. The motion of the front causes the self-reflected wave to be redshifted by the Doppler effect, which in turn serves as an experimentally observable signature for the front propagation. [S0031-9007(96)00202-5]

PACS numbers: 42.65.–k, 41.20.Jb, 42.50.Gy

In the linear optical skin effect a pulse incident from air is reflected from a highly absorbing interface after penetrating only a fraction of a wavelength into the absorbing medium, this distance being the skin depth [1,2]. The skin effect is therefore of fundamental importance in understanding the electrodynamics of pulse propagation at condensed matter interfaces, such as metals for field frequencies below the plasma frequency [2], and semiconductors with highly absorbing excitonic features [3]. In addition, it belongs to an important class of optical problems for which the notion of an electromagnetic field envelope varying slowly on the scale of a wavelength simply does not apply. The skin effect cannot be understood on the basis of envelope equations but is rather a consequence of Maxwell's equations for the interface.

In this Letter we introduce the dynamic nonlinear optical skin effect for pulses and elucidate the underlying physics. In the nonlinear skin effect a high intensity pulse is incident upon a nonlinear absorbing interface. Broadly speaking, saturation of the absorption allows the incident field to penetrate beyond the linear skin depth into the medium, and this causes an absorption front to propagate into the medium which separates the regions of low (saturated) and high (unsaturated) absorption. The front is excited by the incident pulse which is in turn reflected from the sharp absorption front, yielding a self-reflected pulse [4]. Thus the absorption front acts as a moving mirror from which the pulse is self-reflected, and the pulse suffers a redshift due to the Doppler effect [5].

Continuous wave (cw) self-reflection from stationary absorption fronts for plane wave [4] and transverse Gaussian [7] fields incident at sharp and smooth [6] interfaces has been studied theoretically but not experimentally verified so far. In part, this is due to the extremely high absorption and strong saturation required for its manifestation, but the difficulty of obtaining good experimental signatures should not be overlooked. Here we explore the transient regime using the two-level Maxwell-Bloch equations. In particular, we show that moving fronts are excited by the incident pulse [8,9] and that the self-reflected pulse bears clear spectral signatures due to the Doppler effect, which should be observable experimentally.

We consider the time-dependent propagation of a linearly polarized plane electromagnetic wave incident on a nonlinear medium composed of two-level systems. For propagation along the z axis, and taking the electric field polarized along the x axis, Maxwell's curl equations take the form [1,2]

$$\frac{\partial B_y}{\partial t} = -\frac{\partial E_x}{\partial z}, \qquad \frac{\partial D_x}{\partial t} = -\frac{\partial H_y}{\partial z}, \tag{1}$$

where $B_y = \mu_0 H_y$. The specification of the problem is completed with the constitutive relation $D_x = \epsilon_0 E_x + P_x$, where P_x is the optical polarization. To elucidate the basic physics we employ a two-level model to describe the optical response with lower electronic state $|1\rangle$ and upper state $|2\rangle$. The Bloch equations are then (see, for example, Ref. [10])

$$\frac{\partial \rho_{21}}{\partial t} + (\gamma_2 + i\omega_{21})\rho_{21} = i\frac{pE}{\hbar} n,$$
$$\frac{\partial n}{\partial t} + \gamma_1(n - 1) = 2i\frac{pE}{\hbar}(\rho_{21} - \rho_{21}^*), \tag{2}$$

where ρ_{21} is the off-diagonal density matrix element, $n = \rho_{11} - \rho_{22}$ is the population difference between the lower and upper states, ω_{21} is the transition frequency, p is the dipole moment in the field direction, and γ_1 and γ_2 are phenomenological damping constants for the population and polarization, respectively. The polarization due to the atoms is then given by $P_x = N(z)p(\rho_{21} + \text{c.c.})$, with $N(z)$ the density of two-level systems which varies along z in general.

Equations (1) and (2) are solved using a standard discretization scheme described by Yee [11] and the Bloch equations integrated in time using a fourth-order Runge-Kutta method. The system of equations was solved with the initial condition on the field

$$E_x(z, t = 0) = E_0 \cos[2\pi\omega(z - z_0)/c] e^{-(z-z_0)^2/(ct_0)^2}, \tag{3}$$

Vol. 54, No. 3, pp. 774–788, June 1994

010

REFLECTION OF LOCALIZED BEAMS FROM A NONLINEAR ABSORBING INTERFACE *

J. A. POWELL†, E. M. WRIGHT‡, AND J. V. MOLONEY§

Abstract. Beam propagation and reflection are studied at the interface between a Kerr medium and a saturable absorbing nonlinear medium. For spatial solitons propagating nearly tangent to the interface, slowly varying envelope theory describes beam behavior. Phenomena are studied using numerical beam propagation and dynamical systems arguments. Projecting the dynamics onto the soliton modes of the nonabsorbing medium, an effective-particle theory is developed for the reflected beam. The results of the effective-particle theory and the numerical analysis are compared, and a heuristic criterion for predicting reflection and absorption of beams is derived.

Key words. beam reflection, nonlinear optics, effective-particle theory

AMS subject classifications. 78A60, 70K05,58F39, 58F40

1. Introduction.

The reflection properties of nonlinear dielectric interfaces have attracted considerable interest over the last years due to potential applications in all-optical switching [1]–[13]. The basic idea is to understand what adjustable parameters control the reflection of beams at interfaces between optical materials. The angle of beam reflection may be controlled simply by varying the power or phase of an input beam, without changing the incident angle of the input beam. This could result in switching devices that are all-optical, that is, that do not depend on conversion of optical to electric signals, and subsequent slowing of response and loss of information, for switching. In particular, using plane wave theory, Kaplan first predicted bistable reflection, or the possibility of multiple beam reflections dependent on external control parameters, from a linear-nonlinear interface for incidence angles close to the critical angle for total internal reflection [1]. Subsequent numerical simulations using localized beams of finite transverse extent, typically Gaussians, failed to show bistable reflection but exposed several exciting new phenomena such as the nonlinear Goos–Hänchen effect [9], and the transmission of self-focused channels (or solitons) through the dielectric interface [2], [7].

The dynamics of localized beams incident on nonlinear dielectric interfaces was put on a firm theoretical foundation by the introduction of the effective-particle theory by Aceves, Moloney, and Newell [10]. In this theory the incident beam, usually a spatial soliton, is treated as a particle whose motion is dictated by an effective potential that is derived from the linear and nonlinear properties of the interface. Thus, for example, the nonlinear Goos–Hänchen shift can be viewed as critical, slowing down as the particle approaches a turning point of the effective potential.

In this paper we consider the reflection of localized beams from nonlinear absorbing interfaces. Roso-Franco previously showed that for plane waves at normal incidence the nonlinear absorbing interface can display many novel features including bistability and the generation of backward-propagating waves [14]. Here we investi-

* Received by the editors January 25,1993; accepted for publication (in revised form) July 13, 1993. E. M. Wright is partially supported by the Joint Services Optical Program. E. M. Wright and J. V. Moloney are partially supported by Air Force Office of Scientific Research contract FQ8671-9000589 (AFOSR-90-0021).

† Department of Mathematics and Statistics, Utah State University, Logan, Utah 84322-3900 (powell@sunfs.math.usu.edu).

‡ Department of Optical Sciences, University of Arizona, Tucson, Arizona 85721.

§ Department of Mathematics, University of Arizona, Tucson, Arizona 85721.